Separation and Purification Technology 382 (2026) 135596

Contents lists available at ScienceDirect

Separation and Purification Technology

journal homepage: www.elsevier.com/locate/seppur

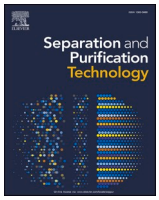

Innovative starch-PVA membranes incorporating amino-functionalized Zeolitic Imidazolate frameworks for CO_2/CH_4 separation

Dalia Refaat [a,b], Jacking Amenakpor [a], Joaquín Coronas [a,b], Beatriz Zornoza [a,b,*]

[a] Instituto de Nanociencia y Materiales de Aragón (INMA), CSIC-Universidad de Zaragoza, Zaragoza 50018, Spain
[b] Chemical and Environmental Engineering Department, Universidad de Zaragoza, Zaragoza 50018, Spain

ARTICLE INFO

Keywords:
Mixed matrix membrane (MMM)
Thin-film nanocomposite (TFN)
Biopolymer membrane
Starch-polyvinyl alcohol (PVA)
Zeolitic Imidazolate framework (ZIF)
amino-functionalized ZIF
CO_2/CH_4 separation

ABSTRACT

The growing need for efficient CO_2 separation in natural gas purification and carbon capture has driven the advancement of high-performance membrane technologies. This study incorporates the zeolitic imidazolate framework ZIF-8-NH_2 into blends of polysaccharide starch and polyvinyl alcohol (PVA) to fabricate eco-friendly membranes. These materials, prepared as dense mixed matrix membranes (MMMs) and thin-film nanocomposite (TFN) membranes, offer a sustainable solution for CO_2/CH_4 separation. The integration of ZIF-8-NH_2 nanoparticles, recognized for their high crystallinity and surface area and selective adsorption capacity into the starch–PVA matrix (33/67 blend ratio), significantly enhances CO_2 permeability, increasing from 124 to 188 Barrer at 10 wt% loading, while preserving high CO_2/CH_4 selectivity (14.1 for the pristine blend and 16.5 for the MMM). For TFNs, a 9/91 starch-PVA matrix with 15 wt% ZIF-8-NH_2 incorporated into the selective layer resulted in the best conditions. This architecture provided robust mechanical stability and high separation performance, yielding a CO_2 permeance of up to 208 GPU and a CO_2/CH_4 selectivity of 26.9 at 3 bar feed pressure, nearly doubling the selectivity compared to the dense biopolymer blend. This work highlights the potential of renewable, starch-based materials in membrane-based gas separation, contributing to sustainable solutions for natural gas purification and carbon capture.

1. Introduction

The efficient separation of carbon dioxide (CO_2) is critical for environmental sustainability and economic viability, particularly in natural gas processing and carbon capture applications. As a major contributor to global warming, CO_2 must be separated from methane (CH_4) to reduce greenhouse gas emissions while simultaneously purifying CH_4 as a clean energy source [1–5]. Membrane technology has emerged as a promising approach for CO_2/CH_4 separation due to its energy efficiency and operational simplicity. Conventional polymeric membranes include materials such as polysulfone (PSF), polyimide (PI), cellulose acetate (CA), and polyetherimide (PEI). These polymers have been widely investigated and utilized due to their intrinsic separation properties, film-forming ability, thermal stability, and relatively good mechanical properties [6]. These membranes face significant challenges in achieving the high permeability and selectivity necessary for industrial applications. To address these limitations, mixed-matrix membranes (MMMs) have been developed, combining the flexibility of polymer matrices with the superior separation capabilities of inorganic fillers [7–9]. This hybrid approach offers a pathway to enhance the gas separation performance of membranes, meeting the stringent requirements of industrial processes. Recent reports have shown that well-designed MMMs can surpass the Robeson upper bound, a key benchmark in membrane science that describes the trade-off between permeability and selectivity [10].

In recent years, sustainable biopolymers such as polysaccharides have gained considerable attention as an environmentally friendly alternative for membrane fabrication. Polysaccharides are derived from renewable natural sources, including plants, algae, and microorganisms, and offer advantages such as biodegradability, biocompatibility, and cost-effectiveness [11]. Among these, starch, a widely available and affordable polysaccharide, has attracted significant interest [11–13]. Starch is the largest natural storage polysaccharide in plants, consisting primarily of amylose and amylopectin, along with minor amounts of lipids and proteins. The properties of starch molecules are influenced by their botanical source, granule morphology, and amylose/amylopectin ratio. Commercial sources of starch include maize, potato, and tapioca. Starch's renewability, biodegradability, and thermoplastic behavior

* Corresponding author at: Instituto de Nanociencia y Materiales de Aragón (INMA), CSIC-Universidad de Zaragoza, Zaragoza 50018, Spain.
E-mail address: bzornoza@unizar.es (B. Zornoza).

https://doi.org/10.1016/j.seppur.2025.135596
Received 29 March 2025; Received in revised form 12 September 2025; Accepted 8 October 2025
Available online 15 October 2025

make it a promising candidate for polymer-based applications [14]. Moreover, the abundance of global starch production estimated at over 80 million metric tons annually offers scalability and economic feasibility for industrial membrane fabrication [15].

Despite these advantages, starch-based membranes face limitations due to their hydrophilic nature and mechanical fragility. To address these challenges, plasticizers such as glycerol and sorbitol are often incorporated to reduce intermolecular forces and improve flexibility [13,16]. However, high plasticizer content can compromise the barrier properties of the polymer, creating a trade-off between mechanical performance and gas separation efficiency. Additionally, starch sensitivity to water activity poses challenges for its use in gas separation membranes. Recent efforts have been made to chemically modify starch or blend it with compatible polymers to enhance its stability and separation performance, yet comprehensive gas separation studies using common starch remain limited [17].

The permeability of starch-based membranes has been extensively studied as a potential alternative to synthetic polymers, particularly for the food industry (packaging and coatings) [18]. **Table S1** presents various applications of starch membranes sourced from different sources and blended with other materials reported in the literature, including water filtration, nanofiltration, hemodialysis, the textile industry, and antibacterial activity. Gas separation was only explored with amino starch[19] and dialdehyde amino-based membranes [20], but not with common starch. This limited exploration suggests a significant research gap that this study aims to address.

Research indicates that the gas permeability of starch, modified starch and plasticized starch membranes is highly dependent on hydration levels [15,21,22]. At low hydration and plasticizer content, starch films exhibit excellent barrier properties, often outperforming conventional materials such as ethylene-vinyl alcohol copolymers and polyamides, which are widely recognized for their superior oxygen barrier performance [23,24]. However, achieving an optimal balance between barrier properties and mechanical performance remains a key challenge [25,26]. While a higher plasticizer content enhances flexibility and processability [11,27], it concurrently reduces barrier efficiency by increasing polymer chain mobility. Additionally, both the mechanical integrity and permeability of starch-based membranes are highly sensitive to moisture levels, making water activity a crucial factor in maintaining their functional stability [15,24,28].

Polyvinyl alcohol (PVA), a biodegradable and water-soluble polymer, is a well-established material in membrane fabrication, offering excellent chemical resistance, mechanical stability and compatibility with starch [11,29]. Crosslinking agents, such as citric acid, are commonly employed to enhance the stability and durability of starch-PVA hybrid membranes [15,21,23]. Citric acid, a cheap, naturally available, non-toxic and biodegradable crosslinker, improves the mechanical and thermal properties of the polymer matrix without introducing harmful additives [11,30]. This modification makes starch-PVA membranes suitable for demanding industrial applications, including gas separation under varying operational conditions. For instance, starch-PVA membranes crosslinked with citric acid have demonstrated improved tensile strength and reduced water uptake, essential for maintaining a consistent performance in humid environments [17,31].

Additionally, zeolitic imidazolate frameworks (ZIFs) into polymer matrices have been shown to significantly boost gas separation efficiency. ZIFs, a category within metal-organic frameworks (MOFs), have distinctive features of high surface area, microporosity and customizable pore structures that enable selective CO_2 adsorption and permeation [1]. The selective affinity of ZIFs for CO_2 over CH_4 makes them ideal for MMM applications targeting the CO_2 separation. Each ZIF variant interacts uniquely with the polymer due to its distinct functional groups and surface chemistries [32,33]. ZIF-8, with the SOD type framework [34,35], increases CO_2 permeability while providing moderate selectivity owing to its neutral surface properties. ZIF-8, featuring a pore size of approximately 0.34 nm, effectively separates CO_2 from methane via two key mechanisms. The first is size exclusion, where the pore dimensions allow smaller CO_2 molecules (kinetic diameter ~ 0.33 nm) to pass through while restricting larger CH_4 molecules (kinetic diameter ~ 0.38 nm). The second mechanism involves selective adsorption, driven by the nitrogen-rich framework of ZIF-8, which preferentially interacts with CO_2 over CH_4. Together, these properties make ZIF-8 a highly efficient material for CO_2/ CH_4 separation [35–38]. Nevertheless, ZIF-8 is susceptible to the gate opening effect, where its framework undergoes subtle structural flexibility under specific conditions, such as gas adsorption or changes in pressure. This transient flexibility can result in a slight, temporary enlargement of the pore dimensions [39]. Despite this phenomenon, ZIF-8 retains its selective performance during CO_2/ CH_4 separation, primarily due to its intrinsic affinity for CO_2 adsorption. Furthermore, By incorporating amino functional groups, ZIF-8-NH_2 facilitates hydrogen bonding interactions with CO_2, leading to enhanced CO_2/CH_4 selectivity compared to the original ZIF-8 structure [1]. ZIF-8-NH_2 retains a similar pore structure, the particle size is approximately 30–50 nm [40] but incorporates functional amino groups. The precise adjustment of pore size (30–50 nm) and chemical functionality in these ZIFs facilitates optimized interactions with CO_2 molecules, driving notable improvements in both CO_2 permeability and CO_2/CH_4 selectivity.

Herein, this study aims to develop novel starch–PVA-based dense MMMs and TFNs, incorporating ZIF-8 and NH_2-functionalized ZIF-8 fillers. Citric acid was employed as a crosslinker exclusively in dense membranes to enhance mechanical stability, while TFNs were fabricated without crosslinking. The integration of ZIFs into a biodegradable polymer matrix was studied in terms of separation efficiency to promote the development of sustainable materials for large-scale applications. By leveraging the synergistic properties of starch, PVA and ZIFs, this research addresses the dual challenges of environmental sustainability and industrial gas separation efficiency, offering a scalable solution to critical environmental and energy challenges.

2. Experimental

2.1. Materials

Polysulfone (Udel® P-3500 LCD) was provided by Solvay Advanced Polymers. Zinc nitrate hexahydrate ($Zn(NO_3)_2{\cdot}6H_2O$), methyl imidazole (mIm), 2-aminobenzimidazole (ambzIm, 97 %), poly[1-(trimethylsilyl) prop-1-yne] (PTMSP) and poly(vinyl alcohol) were bought from Sigma Aldrich, Spain. Soluble potato starch was bought from Laboaragon. The following chemicals were acquired from Análisis Vínicos, Panreac, Labbox, and Scharlab, Spain, in the specified sequence: methanol (MeOH) and isopropanol, *N*-methyl-2-pyrrolidone (NMP), n-hexane, 1-propanol (1-PrOH), and 1-butanol (1-ButOH). The gases required for the separation experiments were obtained from Abelló Linde S.A., Spain. All materials, including solvents, gases, and polymers, were used in their original state without any additional purification steps. All reagents and solvents used were of high purity ($\geq$ 99 %) and were obtained from Sigma-Aldrich and used without further purification.

2.2. Methods

2.2.1. Synthesis of asymmetric PSF supports

The phase inversion technique was employed for the fabrication of PSF supports, following methodologies outlined in prior studies [1,32]. A polymer solution containing 20 wt% PSF in NMP was prepared by stirring thoroughly at room temperature overnight to ensure complete dissolution. The degassed solution was then cast onto a Teflon substrate using an Elcometer 4340 automatic film applicator, forming a film with a thickness of 250 μm at a casting speed of 0.04 m/s. The freshly cast membrane underwent phase inversion by being submerged in a water bath maintained at room temperature for 1 h. Following precipitation, the membranes were rinsed with isopropanol and soaked in deionized

water overnight to eliminate residual solvents. Finally, they were dried in a vacuum oven at 100 °C for 24 h to achieve complete drying and structural stabilization.

2.2.2. Synthesis of ZIF-8

ZIF-8 nanoparticles were synthesized using a modified version of a previously established method [1,32]. For the synthesis process, 1.467 g of $Zn(NO_3)_2{\cdot}6H_2O$ (4.93 mmol) and 3.245 g of 2-methylimidazole (mIm, 39.52 mmol) were separately dissolved in 150 mL of MeOH. The ligand solution was added to the zinc solution while continuously stirring at ambient temperature for 30 min. The mixture was centrifuged at 9000 rpm for 10 min, followed by four consecutive washes with MeOH to eliminate residual impurities. The product obtained was dried and activated by heating at 40 °C overnight to complete the preparation.

2.2.3. Synthesis of ZIF-8-NH_2

ZIF-8-NH_2 nanoparticles were synthesized following a previously reported method [1,41]. To prepare the solution, ambzIm (0.549 g, 4 mmol) and mIm (1.340 g, 16 mmol) were dissolved in 50 mL of methanol (MeOH) and stirred thoroughly at 50 °C for 2 h, resulting in a clear solution. Meanwhile, $Zn(NO_3)_2{\cdot}6H_2O$ (0.75 g, 2.5 mmol) was dissolved in a separate 50 mL of MeOH. After cooling the clear mixed-linker solution to room temperature (23 °C), the Zn-containing solution was introduced, and the mixture was stirred for 1.5 h, producing a milky suspension. The suspension was centrifuged at 2500 rpm for 30 min, washed three times using fresh MeOH, and dried under vacuum at 80 °C for 12 h. A final drying step was conducted at 150 °C for 1 h.

2.2.4. Preparation of dense mixed matrix membranes

A 10 % (*w/v*) PVA solution in water (50 mL) was prepared in a beaker. Separately, a 5 % (w/v) starch dispersion was made by heating starch in water at 100 °C. Once the starch dispersion was ready, it was added dropwise to the PVA solution under constant stirring to achieve a homogeneous mixture [42]. Citric acid (CA) was added to this mixture at a concentration of 2 wt% while ensuring continuous stirring and avoiding the incorporation of air bubbles. The resulting blend was cast into a membrane using the conventional solution casting method. After casting, the membrane was washed thoroughly with distilled water to remove any traces of CA. Finally, the membrane was air-dried at room temperature, obtaining a transparent, dense film with a thickness ranging from 50 to 60 μm. The fabricated membranes were labeled as D. ST-X% where X represents the ST/PVA composition in wt%. To fabricate dense MMM membranes incorporating ZIF nanocrystals, the optimal conditions identified for dense membranes in gas separation experiments were utilized. The polymer was initially dissolved in 2/3 of the total solvent volume under stirring at 80 °C. In parallel, ZIF particles, ranging from 5 to 15 wt% relative to the total MMM composition, were dispersed in the remaining 1/3 of the solvent using an ultrasonic bath to ensure an even distribution. After the polymer was completely dissolved and cooled to 40–45 °C, the ZIF suspension was gradually introduced and mixed thoroughly to form a homogeneous solution. The ZIF-containing mixtures were stirred at 45 °C for 1 h before the casting process. The fabricated membranes were labeled as MMM ST/PVA-ZIF-8-NH_2-Y%, where Y represents the ZIF loading in wt%. The resulting blend was cast into a membrane using a Petri dish. After casting, the membrane was washed thoroughly with distilled water to remove any traces of CA. Finally, the membrane was air-dried at room temperature obtaining MMM membranes.

2.2.5. Preparation of TFC and TFN membranes

The thin-film composite (TFC) and thin-film nanocomposite (TFN) membranes were prepared following a previously reported study [32]. To prevent the selective layer from infiltrating into the PSF supports, a PTMSP gutter layer was applied via spin-coating. A 2 wt% PTMSP solution was prepared by dissolving the polymer in n-hexane at room temperature. The PSF support was securely fixed on the spin coater (Model WS-650MZ-23NPP/A1/AR1) and 0.7 mL of the PTMSP solution was evenly spread by spinning at 2500 rpm for 20 s. The coated supports were then dried in an oven at 40 °C for 1 h to remove any residual solvent.

The selective layer, consisting of a starch/PVA mixture, was deposited on the PTMSP-coated PSF supports. To prepare the selective layer solution, starch and PVA were individually dissolved in distilled water and then combined in equal volumes (1,1 *v*/v) before stirring continuously at 80 °C for 2 h. A 0.6 mL aliquot of this solution was applied to the PTMSP/PSF supports through spin-coating at 2500 rpm for 20 s. The final multilayer structure, comprising starch/PVA/PTMSP/PSF, was designated as the TFC membrane. The fabricated TFC membranes were labeled as TFC-ST-X%, where X represents the ST/PVA composition in wt%.

To fabricate TFN membranes incorporating ZIF nanocrystals, the optimal conditions identified for TFC membranes in gas separation experiments were utilized. The polymer was initially dissolved in 2/3 of the total solvent volume while maintaining temperature and stirring. In parallel, ZIF particles, ranging from 5 to 15 wt% relative to the total MMM composition, were dispersed in the remaining 1/3 of the solvent using an ultrasonic bath to ensure an even distribution. After the polymer was completely dissolved and cooled to 40–45 °C, the ZIF suspension was gradually introduced and mixed thoroughly to form a homogeneous solution. The ZIF-containing mixtures were stirred at 45 °C for 1 h before the spin-coating process. The fabricated membranes were labeled as TFN ST/PVA -ZIF-8-NH_2-Y%, where Y represents the ZIF loading in wt%. Following the spin-coating step, the membranes were dried at 40 °C for 18 h to ensure the complete removal of residual solvents.

2.3. Characterization of ZIFs and membranes

The morphology of ZIF powders and membranes was examined using scanning electron microscopy (SEM) with an FEI Inspect F50 instrument operating at 10 kV. The SEM was also employed to measure the thickness of the selective skin layer at 5–6 locations across the membrane. For cross-sectional imaging, membrane samples were freeze-fractured in liquid nitrogen and coated with a palladium layer before analysis. Thermogravimetric analysis (TGA) was performed using a Mettler Toledo TGA/STDA 851e system. Approximately 3 mg of ZIF powder was placed in 70 mL alumina pans and subjected to heating from 35 to 700 °C at a controlled rate of 10 °C min^{-1}, with a N_2 flow of 40 cm^3 (STP) min^{-1}. Fourier transform infrared (FTIR) spectroscopy was conducted using a Bruker Vertex 70 instrument equipped with a Golden Gate diamond ATR attachment and a DTGS detector. Spectra were recorded in the range of 4000–600 cm^{-1} with a resolution of 4 cm^{-1}, averaging 60 scans for each sample. Crystallinity was assessed through X-ray diffraction (XRD) analysis using a Panalytical Empyrean system with CuKα radiation (λ = 0.154 nm). Scans were performed over a 2θ range of 5° to 40° at a step size of 0.03° s^{-1}.

2.4. Gas separation tests

Membrane samples with active areas of 2.12 cm^2 for TFC/TFN membranes and 12.57 cm^2 for dense membranes were tested in a permeation module composed of two stainless steel components. The membranes were supported by a 316LSS macro-porous disk (Mott Co., 20 μm nominal pore size) and sealed using Viton O-rings. Temperature control at 35 °C was maintained by placing the module in a UNE 200 Memmert oven. The separation performance was evaluated by feeding a CO_2/CH_4 gas mixture (50/50 cm^3 (STP) min^{-1}) to the membrane's feed side at 3 bar pressure. Gas flow was regulated using Alicat Scientific MC-100CCM-D mass flow controllers. On the permeate side, helium at a flow rate of 4.5 cm^3 (STP) min^{-1} was used as a sweep gas at atmospheric pressure (~1 bar), controlled by an Alicat Scientific MC-5CCM-D controller. The stage cut (θ), representing the permeate-to-feed flow

rate ratio, was maintained at approximately 1 %. Gas composition on the permeate side was monitored in real time using an Agilent 3000 A micro-gas chromatograph. Steady-state conditions were ensured before calculating the permeability/permeation parameters for CO_2 and CH_4. Permeability is expressed in Barrer (10^{-10} cm^3(STP)·cm·cm^{-2} s^{-1} $cmHg^{-1}$) for dense and permeation in GPU (gas permeance unit, 10^{-6} cm^3 (STP) cm^{-2} s^{-1} $cmHg^{-1}$), for TFC/TFN membranes. Permeability involves flux (flow rate divided by the area of the membrane), partial pressure, and multiplying by the membrane thickness (Eq.1).

The gas permeance was calculated by dividing the N is molar flow rate of the permeate gas by the membrane area (A) and partial pressure difference of the permeating gas (ΔP) across the membrane (Eq.2.) The CO_2/CH_4 selectivities were determined as the ratio of their respective experimental permeabilities and permeances, respectively (Eq.3). The permeance was calculated using the measured gas flux, membrane area, and feed and permeate partial pressures of permeating gases. Measurements were repeated on three membrane samples under identical conditions and average values along with associated errors were recorded for each membrane.

$$P_{gas}(\text{Barrer}) = \frac{\text{Flux}_{gas}\ (cm^3(STP)\cdot cm^{-2}\cdot s^{-1})\cdot \text{Thickness (cm)}}{\Delta P_{gas}\ (\text{cmHg})} \quad (1)$$

$$\text{Permeance (GPU)} = \frac{N\ (cm^3(STP)\cdot s^{-1})}{\Delta P(cmHg).A(cm^{-2})} \quad (2)$$

$$\alpha = \frac{P_{CO2}}{P_{CH4}} \quad (3)$$

3. Results

3.1. Characterization of ZIF-8 & ZIF-8- NH_2

ZIF-8 and ZIF-8-NH_2 nanoparticles were synthesized for application as fillers in starch-PVA MMM and TFN membranes. The ZIF-8 and ZIF-8-NH_2 average particle sizes are 78 nm ±6 and 52 ± 5 nm, respectively, as illustrated in Fig. 1.

Thermogravimetric analysis (TGA) was carried out under N_2 atmosphere, spanning a temperature range of 35 to 700 °C. The results, plotted in Fig. 2a, indicate that the synthesized ZIF particles undergo decomposition between 200 and 700 °C. ZIF-8 was found to degrade at a higher temperature, around 450 °C, whereas ZIF-8-NH_2, which contains a modified ligand structure, remained thermally stable up to 400 °C. This stability suggests that ambzIm is integrated into the ZIF-8 framework through coordination with the metal ions, rather than being physically trapped within the porous structure[40].

The crystallinity and purity of the ZIF particles were confirmed through X-ray diffraction (XRD) analysis, with the corresponding results presented in Fig. 2b. ZIF-8 and ZIF-8-NH_2 characteristic diffraction peaks were observed at 2θ = 7.3°, 10.4°, 12.7°, 14.8°, 16.4°, 18.0°, 24.5°, and 26.1°, which correspond to the planes (011), (002), (112), (022), (013), (222), (114) and (134), in good agreement with earlier findings and confirming the SOD type structure of ZIF-8 [35]. XRD analysis demonstrated that the substitution of the mIm linker in ZIF-8 with the ambzIm linker, a primary amine-functionalized imidazole ligand, in ZIF-8-NH_2 maintained the structural integrity of the original crystal framework, aligning with previous reports [1,40,43]. Interestingly, the produced ZIF-8-NH_2 nanocrystals exhibited lower particle sizes (refer to Fig. 1) and the XRD patterns exhibited reduced peak intensities for the modified material compared to the original ZIF-8 nanocrystals. This decrease could be attributed to the incorporation of bulkier ligands during the exchange process, which introduce steric hindrance effects, potentially causing structural imperfections or distortions.

As shown in Fig. 2c, the FTIR-ATR spectrum of ZIF-8 lacks the characteristic bands at 1147 cm^{-1} and 993 cm^{-1}, associated with the C—N bond, confirming the effective ligand exchange. In the case of ZIF-8-NH_2, new peaks appear at 3470/3385 cm^{-1} and 916/848 cm^{-1}, corresponding to –NH_2 and –NH– groups, respectively. These spectral features provide additional evidence that the ambzIm linker successfully replaced the mIm linker in the ZIF-8 structure [40].

3.2. Characterization of dense starch membranes

Fig. 3 shows the SEM cross-sectional images of starch (ST)-polyvinyl

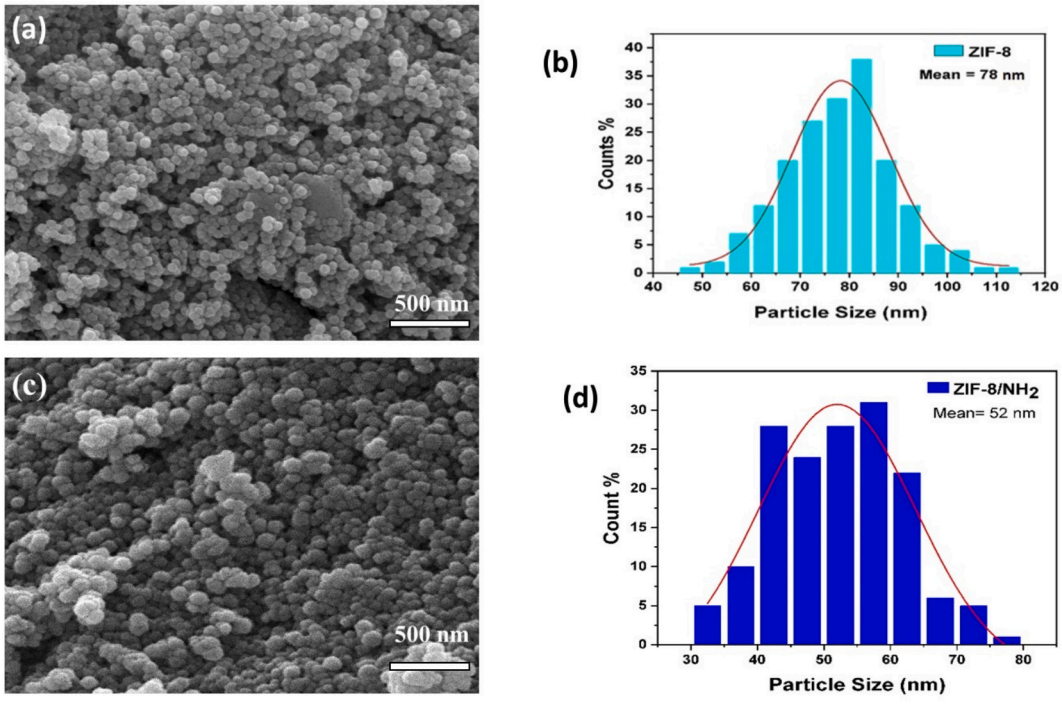

Fig. 1. Particle size of ZIF nanoparticles. ZIF-8: SEM image (a) and histogram (b); ZIF-8-NH_2: SEM image (c) and histogram (d).

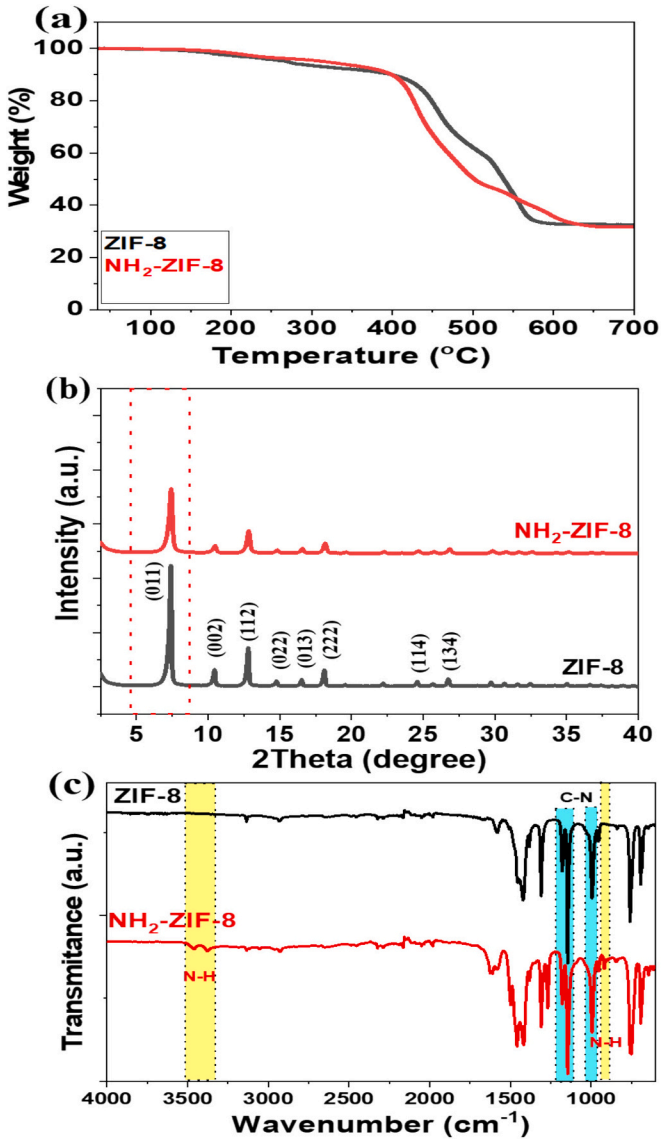

Fig. 2. ZIF powders: TGA curves in N_2 (a), XRD patterns (b) and ATR-FTIR spectra (c).

alcohol (PVA) mixed matrix membranes (MMMs) with citric acid (CA) as a crosslinker, examining the structural variations in the membrane based on the starch content and the presence of ZIF-8-NH_2 (10 %) as an additive. The images in Fig. 3**(a-d)** provide some insights into how different compositions of starch (0–100 wt%).

affect the morphology of these membranes. Fig. 3a shows the cross-section SEM image of a membrane composed entirely of starch (D.ST-100, Table 1), crosslinked with citric acid. The structure appears dense and homogeneous, indicating a uniform starch matrix without visible pores or phase separation, which provides limited permeability but strong barrier properties. However, when submitted to the gas separation set up the membrane was too brittle to test. In Fig. 3b (D.ST-33 of Table 1), which includes both starch and PVA, the cross-section reveals a more porous and textured structure compared to the bare starch membrane. The addition of PVA and the lower starch content creates a morphology with greater porosity, which potentially enhance CO_2 permeability. The presence of citric acid as a crosslinker maintains the mechanical stability despite the more open structure. Fig. 3c corresponds to the bare PVA membrane (D.ST-0 of Table 1), pure PVA with citric acid without starch. The SEM image shows a dense and compact morphology, characteristic of PVA's cohesive film-forming properties. The absence of starch results in a smooth cross-sectional structure, which restricts gas permeability but keeps selectivity and improves mechanical integrity. The crosslinking with citric acid likely enhances the membrane's structural resilience. Fig. 3d shows the cross-section of MMM ST-33-ZIF-8-NH_2 (10 wt%), which contains a blend of starch and PVA with 10 % ZIF-8-NH_2 particles, demonstrating a heterogeneous morphology. The incorporation of ZIF-8-NH_2 particles provokes visible textural changes, creating microdomains within the polymer matrix. These particles, known for their high specific surface area and CO_2 affinity, produced an enhancement of the membrane gas separation properties by facilitating CO_2 transport through the matrix, as shown in Table 1. Citric acid crosslinking in this formulation enhances the mechanical strength of the membrane. Furthermore, SEM-EDS analysis was performed to gather additional details about the samples. **Fig. S1** and **Table S2** exhibit the elemental composition of MMM ST-33-ZIF-8-NH_2 (10 wt%). The Zn mapping indicates a uniform distribution of MOF particles within the surface of ST/PVA MMMs, confirming a successful interaction between ST/PVA and the MOFs.

Fig. 4 represents the ATR-FTIR spectra for dense starch/PVA membranes and ZIF MMMs. The D.ST-0 membrane (as shown in Table 1) spectrum displays a broad peak around 3300 cm^{-1}, attributed to the O—H stretching vibrations, which is characteristic of the hydroxyl groups in PVA. Other notable peaks include the C—H stretching near 2900 cm^{-1} and a weaker peak at around 1700 cm^{-1} due to the C═O stretching, which arise from the oxidation of PVA during processing. The dense starch membrane spectrum (D.ST-100) also exhibits a broad O—H stretching peak around 3300 cm^{-1}, indicative of hydrogen bonding between the starch chains, with additional peaks corresponding to C—O and C—H stretching vibrations, characteristic of the starch polysaccharide structure [44]. In the starch/PVA blend membrane 33/67 (D.ST-33) spectrum, the overlapping broad O—H stretching band around 3300 cm^{-1} and the C—H stretching near 2900 cm^{-1} indicate that the matrix combines both starch and PVA properties. Slight shifts in these peaks suggest hydrogen bonding interactions between starch and PVA, enhancing the stability and compatibility of the blended polymer matrix [18,44].

Fig. 4 also shows the MMMs incorporating ZIF-8-NH_2 at 5, 10 and 15 wt% loadings exhibiting notable new peaks or changes in the existing peaks, signifying the presence and influence of ZIF-8-NH_2 within the polymer matrix. For instance, a peak around 1550 cm^{-1} corresponds to the C═N stretching vibration of the imidazole ring in ZIF-8 [1], confirming its integration within the polymer network. Additionally, the peaks below 1000 cm^{-1} are associated with metal-ligand vibrations, further indicating the presence of the ZIF-8 structure within the polymer network. As the ZIF-8-NH_2 content increases from 5 to 15 wt%, the C═N stretching peak around 1550 cm^{-1} becomes more pronounced, along with the increased intensity of the metal-ligand peaks below 1000 cm^{-1}. Moreover, the O—H stretching region (3300 cm^{-1}) shows a reduced intensity as the ZIF-8 content rises. Besides, incorporating ZIF-8-NH_2 into the starch/PVA matrix introduces functional amino groups (−NH_2) that can form hydrogen bonds with the hydroxyl groups (-OH) of starch. These interactions are crucial in establishing strong interfacial bonding between the filler and the polymer matrix, affecting the structural and functional characteristics of the membrane. The hydrogen bonding between the amino groups of ZIF-8-NH_2 and the hydroxyl groups of starch enhances their mutual compatibility. It reduces the formation of interfacial voids, ensuring a better dispersion of ZIF-8-NH_2 particles within the matrix, as compared to ZIF-8, where such a possibility does not exist. This bonding likely restricts the mobility of the polymer chains, leading to a more rigid matrix with reduced free volume. Such structural modifications improve the gas separation performance by creating a more selective pathway for CO_2 molecules while limiting CH_4 transport.

Fig. 5 and **Fig. S2** illustrate the thermogravimetric analysis (TGA) curves, which show the thermal stability profiles of different starch/PVA-based membranes and MMMs. All samples exhibit two primary stages of weight loss, consistent with the typical thermal decomposition

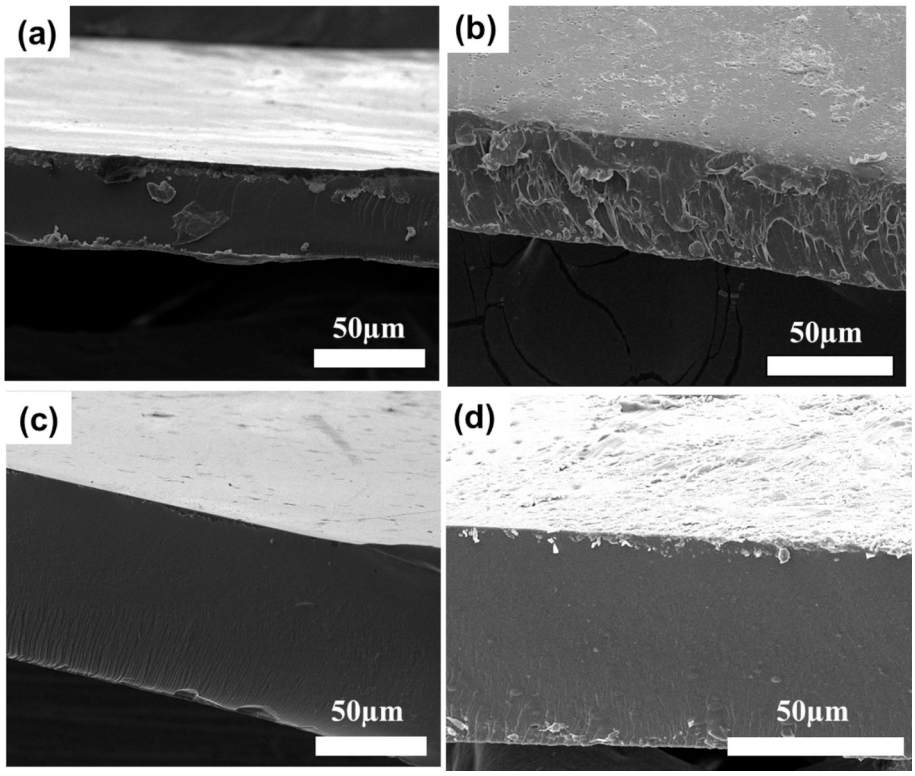

Fig. 3. SEM cross-sections for starch (ST)-PVA membranes & MMM: D.ST-100 (a), D.ST-33 (b), D.ST-0 (c) and MMM ST-33-ZIF-8-NH_2 (10 wt%) (d).

Table 1
CO_2/CH_4 mixture separation performance for starch/PVA membranes with different starch/PVA composition (0/100 to 100/0) and MMM membranes with a range of loadings (5–15 wt%) of ZIF-8-NH_2 fillers and 10 wt% for ZIF-8 filler. Crosslinker concentration was set at 2 wt%. For the optimal ST/PVA composition (33/67). the variation from 1 to 3 wt% of the total starch/PVA blend is studied.

Membrane sample	ST/PVA Composition	Citric acid (wt%)	PCO_2 (Barrer)	PCH_4 (Barrer)	$S(CO_2/CH_4)$	CO_2 Purity (%)	CO_2 Recovery (%)
D.ST-0	0/100	2	59.4 ± 19.5	4.8 ± 1.7	12.6 ± 0.3	92.7	0.023
D.ST-9	9/91	2	55.6 ± 4.0	5.3 ± 0.4	10.5 ± 0.1	91.3	0.021
D.ST-17	17/83	2	66.0 ± 4.7	7.2 ± 3.5	11.5 ± 1.0	92.0	0.025
D.ST-23	23/77	2	71.4 ± 7.7	5.1 ± 1.6	14.9 ± 0.4	93.7	0.027
D.ST-29	29/71	2	120.3 ± 8.2	8.5 ± 0.7	14.1 ± 0.5	93.4	0.046
		1	58.1 ± 2.2	5.8 ± 0.2	10.0 ± 0.7	90.9	0.022
D.ST-33	**33/67**	**2**	**123.7 ± 3.0**	**8.8 ± 0.3**	**14.1 ± 0.4**	93.4	0.047
		3	74.6 ± 6.2	3.9 ± 1.6	19.2 ± 0.8	95.1	0.028
D.ST-50	50/50	2	117.6 ± 3.8	11.0 ± 0.3	10.7 ± 0.7	91.5	0.044
D.ST-75	75/25	2	78.6 ± 3.4	6.7 ± 0.2	11.7 ± 0.3	92.1	0.030
D.ST-100	100/0	2	–	–	–	–	–
MMM ST-33-ZIF-8-NH_2 (5 wt%)	33/67	2	195.9 ± 13.6	14.9 ± 3.3	13.1 ± 0.1	92.9	0.074
MMM ST-33-ZIF-8-NH_2 (10 wt%)	**33/67**	**2**	**188.1 ± 16.5**	**18.5 ± 5.8**	**16.5 ± 1.5**	94.3	0.071
MMM ST-33-ZIF-8-NH_2 (15 wt%)	33/67	2	135.1 ± 0.3	10.5 ± 0.6	12.9 ± 0.1	92.8	0.051
MMM ST-33-ZIF-8 (10 wt%)	33/67	2	45.28 ± 15	3.5 ± 1.4	13.2 ± 1.8	93.0	0.017

* Pure ST-dense membranes are inherently brittle, contributing to mechanical fragility, which leads to membrane failure during testing. In all case, the dense membranes thickness range 50–60 µm.

behavior of starch and PVA. The initial weight loss occurs at around 100 °C, attributed to the removal of adsorbed water due to the hydrophilic nature of both starch and PVA. This is followed by a more significant weight loss at higher temperatures, which is indicative of polymer decomposition. The dense ST- 0 membrane begins to decompose at around 250 °C and shows a significant degradation around 300–400 °C. This thermal behavior is typical of PVA, as it breaks down through the dehydroxylation and chain scission of polymer backbones. The curve corresponding to the starch/PVA blend (D.ST-33) membrane shows an initial weight loss at a slightly lower temperature than pure PVA, which aligns with the more thermally sensitive nature of starch.

The MMMs containing ZIF-8-NH_2 demonstrate significantly improved thermal stability compared to pure starch/PVA membranes, particularly with ZIF-8-NH_2. The inclusion of ZIF-8-NH_2 delays the onset of major weight loss, as observed in the 5, 10, and 15 wt% loaded membranes, suggesting an enhanced thermal resistance. Among these, the 5 wt% ZIF-8-NH_2 membrane achieves the greatest thermal stability, highlighting the role of ZIF-8-NH_2 in reinforcing the polymer matrix. This improvement can be attributed to the high thermal resistance and structural integrity of ZIF-8-NH_2 particles, which act as heat barriers and slow down the polymer decomposition. However, at higher temperatures, the thermal stability decreases due to the catalytic effect of Zn-based particles present in ZIF-8-NH_2[45]. When ZIF-8-NH_2 degrades into ZnO during its thermal decomposition, such oxide acts as a catalyst,

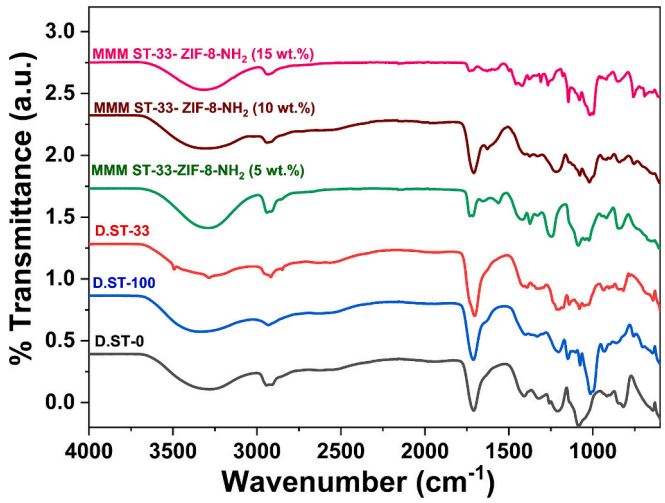

Fig. 4. ATR-FTIR spectra of starch/PVA membranes and ZIF-8-NH_2MMMs.

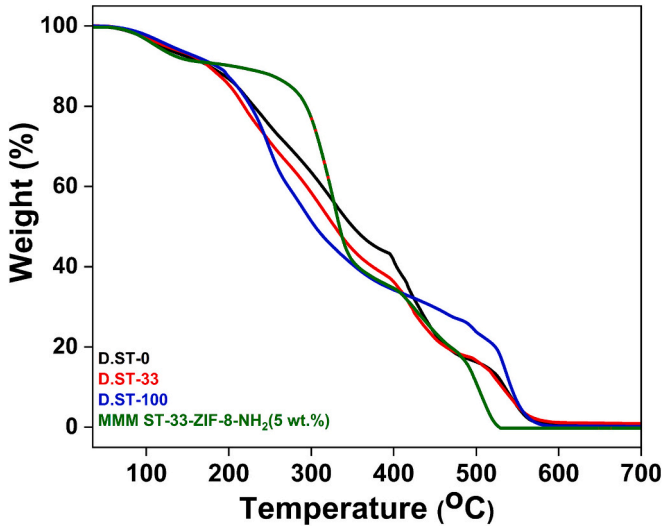

Fig. 5. TGA curves in N_2 of starch/PVA membrane and ZIF-8-NH_2 MMMs.

accelerating the breakdown of the polymer matrix. This catalytic effect becomes more prominent with increased ZIF-8-NH_2 content, as shown in the weight loss profiles and the earlier degradation temperatures of the composite membranes compared to the pure starch/PVA materials [45,46]. Thermogravimetric analysis confirmed that there is a slight loss of most likely water below 100 °C. Above ~100 °C, the degradation event was consistent with the thermal decomposition of starch and PVA. It is worth noting that the membranes are conditioned in-situ in the gas separation setup. If not, such water is probably removed by gas separation tests with dry gases and steady state reached after at least 2 h of measurements.

Fig. 6 illustrates the XRD patterns for the different starch/PVA-based membranes and MMMs. The XRD pattern for the starch-PVA blend shows a broad, amorphous hump around 2θ equal to 20°, indicative of its semi-crystalline nature [47,48]. This characteristic peak is commonly associated with the disordered arrangement of polymer chains in blended biopolymers such as starch and PVA. The XRD analysis confirms the successful incorporation of ZIF-8-NH_2 into the starch/PVA polymer matrix, as evidenced by the characteristic peaks at 2θ 7.3°, 10.4° and 12.7°, corresponding to the crystalline structure of ZIF-8-NH_2. The intensities of these peaks increase with higher filler content, indicating proportional integration and preservation of the MOF structure upon the

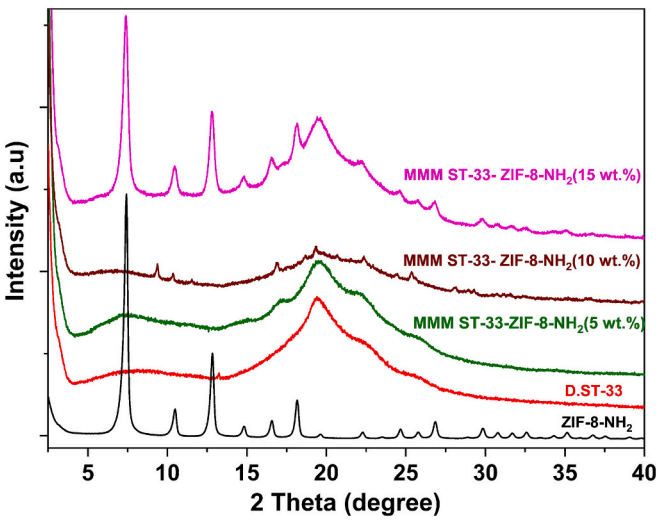

Fig. 6. XRD patterns of starch/PVA membrane and ZIF-8-NH_2 MMMs.

process of MMM fabrication. Notably, the 15 wt% sample shows more prominent peaks compared to the 10 wt% sample, which has smaller peaks possibly due to minor filler aggregation or the formation of secondary phases. In contrast, no significant peaks are observed in the 5 wt % sample, likely because the ZIF-8-NH_2 is well-dispersed and embedded within the polymer matrix, making it undetectable by XRD. Additionally, the incorporation of ZIF-8-NH_2 reduces the amorphous nature of the polymer, enhancing rigidity and structural integrity, particularly at higher filler content (15 wt%) [1,47–50].

3.3. CO_2/CH_4 separation performance

Table 1 shows the different starch/PVA blending membranes prepared with their codes and compositions.

The gas separation efficiency of the dense starch/PVA membranes prepared with different starch concentrations (0–75 wt%) was evaluated using a 50:50 CO_2/CH_4 mixture at a feed pressure of 3 bar and 35 °C. As depicted in Table 1 and Fig. 7a, the gas separation performance (CO_2 and CH_4 permeabilities and CO_2/CH_4 selectivity), increasing the starch content positively influences the CO_2 permeability (from 59.4 to 123.7 Barrer), which is attributed to the inherent properties of starch that contribute to the formation of a more porous and CO_2-philic structure. This enhanced permeability can be linked to the increased free volume and amorphous regions within the starch/PVA blend, facilitating a greater CO_2 transport [51–53]. The CO_2/CH_4 selectivity also shows an increasing trend with higher starch content (from 10.5 to 14). This improvement in selectivity is due to the preferential interaction between CO_2 molecules and the hydroxyl groups present in the starch, which promotes the CO_2 adsorption over that of CH_4. The high density of polar groups within the starch structure enhances the solubility selectivity due to the preferential interaction with the quadrupole to the CO_2 molecule, aligning with findings from previous research that reported similar behavior in polysaccharide-based membranes [51,54]. In Table 1 and Fig. 7b, the effect of citric acid concentration (1–3 wt%), as a crosslinker agent on the gas separation performance, is illustrated. Citric acid is known for its ability to form covalent crosslinks between polymer chains having hydroxyl groups, enhancing mechanical stability and reducing excessive swelling in humid conditions [55–57]. Fig. 7b indicates that, as the citric acid concentration increases, the CO_2 permeability initially rises but slightly decreases beyond the 2 wt% value. This behavior can be attributed to the optimal crosslink density achieved at this concentration, which balances permeability and selective gas transport [58]. Specifically, the permeability of dense membranes reached its maximum at 2 wt% of citric acid and then slightly decreased

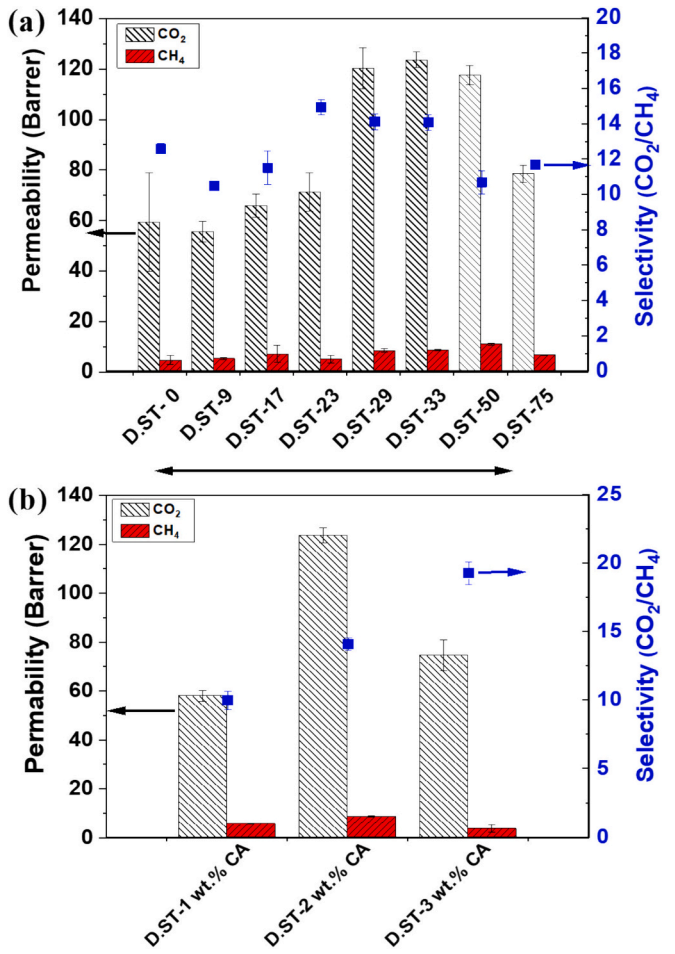

Fig. 7. CO_2/CH_4 separation performance with the dense membranes fabricated at different starch concentrations (a), and different concentrations of cross-linker (1–3 wt%) (b).

with further loading, while the CO_2/CH_4 selectivity continued to increase with higher citric acid content. This trend is consistent with the expected decrease in permeability of dense polymeric membranes [10,52]. At the same time, the CO_2/CH_4 selectivity showed a slight increase with increasing citric acid concentration. The cross-linking effect restricts the polymer chain mobility and enhances the sieving effect, which favors smaller CO_2 molecules over CH_4 due to differences in their kinetic diameters. Too much crosslinking in the gas transport channels causes a decrease in the CO_2 permeability (probably due to the excessive densification of the polymer structure achieved) without significantly affecting the CO_2/CH_4 selectivity.

After studying the separation performance of the bare polymer, the MMMs incorporating ZIF-8-NH_2 and ZIF-8 were studied. The CO_2 permeabilities and CO_2/CH_4 selectivities of dense membranes with 33/67 ST/PVA blending composition (D.ST-33) and those containing 5, 10 and 15 wt% of ZIF-8-NH_2 are compared in Fig. 8 and Table 1. As expected, the incorporation of ZIF-8-NH_2 at different amounts noticeably affected the CO_2/CH_4 separation performance of MMMs compared to the bare polymer membrane. Membranes with 5 wt% of ZIF-8-NH_2 resulted in a significant increase in CO_2 permeability (from 123 to 196 Barrer), indicating an enhanced gas transport facilitated by the well-dispersed ZIF-8-NH_2 nanoparticles. The amino-functionalized surface provides strong affinity sites for CO_2, supporting more efficient sorption and selective diffusion mechanisms [1,59]. At 10 wt% filler loading, CO_2 permeability slightly decreases to 188 Barrer. This trend could be attributed to partial aggregation of ZIF-8-NH_2 particles, which limits the available free volume and disrupts gas transport channels [60]. At 15 wt

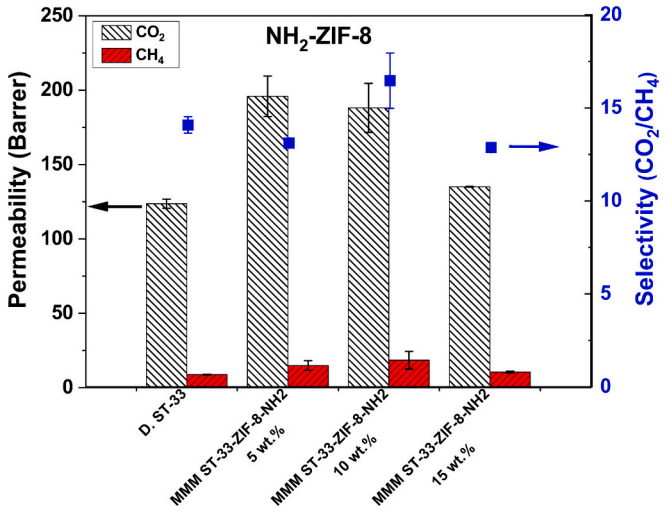

Fig. 8. CO_2/CH_4 separation performance of starch/PVA MMMs with 5–15 wt% ZIF-8-NH_2.

% loading, the further reduction in CO_2 permeability (136 Barrer) and selectivity obtained indicates an excessive filler content leading to aggregation, causing non-selective voids or defects within the polymer matrix. Such aggregation impedes efficient gas transport. This phenomenon has been corroborated by various studies on MMMs incorporating MOF-type fillers [61,62]. The best value of CO_2/CH_4 selectivity (16.5) observed at the 10 wt% ZIF-8-NH_2 content, without a sacrifice in the CO_2 permeability (Fig. 8) is likely due to optimal interfacial compatibility achieved between the polymer matrix and filler particles. Moreover, the –NH_2 groups on the ZIF-8 surface create favorable interactions with CO_2 molecules, enhancing selective adsorption and transport [63].

Concerning the MMMs containing 10 wt% ZIF-8 loading (i.e., with the non-functionalized MOF), they showed a reduced CO_2 permeability of 45 ± 15 Barrer together with a CO_2/CH_4 selectivity of 13.2 ± 1.8 (as shown in Table 1). These values are worse than those achieved with the amino MOF. The larger particle size of ZIF-8 (78 nm) limits its dispersion within the polymer matrix, leading to uneven distribution and suboptimal gas transport channels. Its lack of functional groups, such as amines, weakens the CO_2-specific interactions, reducing the adsorption affinity and thus separation selectivity compared to ZIF-8-NH_2, which benefits from amino-functionalized surfaces that enable acid-base interaction with CO_2 molecules. The weak interfacial bonding between ZIF-8 and the polymer matrix further results in defects and voids, compromising the mechanical and separation performance. In sum, NH_2-ZIF-8, with a smaller particle size (52 nm) and better compatibility and interaction with CO_2 molecules, achieves improved dispersion and interaction with the polymer matrix, leading to superior permeability and selectivity. The 10 wt% ZIF-8-NH_2 MMMs exhibited, in turn, the best separation performance in comparison to the pristine starch/PVA (33/67 %) and the other MMMs. This enhancement can be attributed to the creation of preferential pathways for CO_2 transport within the crystalline structure of ZIF-8-NH_2, which is critical for improving gas separation performance [64]. In addition, the hydrogen bonding interactions of the –NH_2 groups on the ZIF-8 also contribute to optimizing the sorption-diffusion mechanism within the membrane. By moderating CO_2 sorption and promoting a selective transport environment, the functionalized matrix achieves a balance between permeability and selectivity, showcasing the potential of ZIF-8-NH_2 as an effective filler in mixed-matrix membranes. This fine-tuning of the polymer-filler interface is key to advancing the design of high-performance membranes for gas separation applications [65,66].

Additionally, the CO_2 purity, calculated by excluding the He sweep gas contribution and considering only the CO_2/CH_4 ratio in the

permeate stream, ranged from 90.9 to 95.1 % for dense ST/PVA membranes as in Table 1 and 77.3–96.4 % for TFC/TFN membranes as in Table 2. The highest purity values (>95 %) were achieved by citric acid-crosslinked dense membranes (D.ST-33 with 3 % CA) and ZIF-8-NH_2-incorporated TFN membranes, demonstrating the effectiveness of both chemical crosslinking and porous filler strategies for enhancing selectivity [67].

The CO_2 recovery, calculated as the fraction of CO_2 permeated relative to the CO_2 fed, showed distinct trends between membrane types. Dense ST/PVA membranes exhibited recoveries of 0.017–0.074 %, while TFC/TFN membranes achieved 0.033–0.221 %. Notably, the TFN ZIF-8-NH_2 series showed higher recovery than dense membranes at comparable purity levels (>92 %), attributable to their superior CO_2 permeance. This enhancement stems from the combined effects of molecular sieving through ZIF-8 pores and facilitated transport via NH_2-CO_2 interactions [67,68].

3.4. Characterization and separation performance of TFC and TFN membranes

After studying the preparation of dense membranes, TFC and TFN were prepared with the best-performing filler ZIF-8-NH_2. Fig. 9 presents the cross-section SEM images for starch/PVA TFC and TFN membranes showing the morphological changes induced by varying the polymer concentration in the casting solution. Moreover, as shown in Fig. 9, a thin starch/PVA coating (1–1.5 μm) was applied over the PSF support membrane, separated by a PTMSP gutter layer. This design prevents the starch/PVA from penetrating the PSF support, avoiding potential increases in transport resistance that hinder gas separation performance [69]. As a highly permeable and minimally selective material, the PTMSP polymer is likely to have a negligible effect on the total gas permeation resistance [70]. Based on the gas separation performance results represented in Table 2 and **Fig. S5a**, the most effective casting solution consists of a 9 wt% concentration of starch/PVA (TFC-ST-1 %) (212 GPU of CO_2 with a CO_2/CH_4 selectivity of 17.3, discussed below), which was then applied for further examination in the fabrication of ZIF-8-NH_2 based TFN membranes, as shown in Fig. 9. The figure displays SEM images of TFN membranes incorporating ZIF-8-NH_2 particles at 5, 10, and 15 wt% loadings, showcasing the PSF porous support, the starch/PVA thin film layer, and the dispersed filler particles. The results reveal that the ZIF-8-NH_2 particles were effectively embedded into the starch/PVA polymer matrix, which was deposited onto the PSF support to form the TFN membranes. The particles exhibited uniform dispersion across the surface, with no noticeable aggregation on the top layer of the membranes, confirming the successful interaction between ST/PVA and the MOFs. Corroborating this, **Fig. S3** and **Table S3** exhibit the elemental composition of ZIF-8-NH_2 in TFN ST/PVA −10 wt% with a uniform distribution of Zn.

The XRD patterns presented in **Fig. S4** for the TFC and TFN membranes, prepared with 5, 10, and 15 wt% loadings, exhibit a broad and weak peak centered around $2\theta \approx 15–22^\circ$. This peak reflects the low crystallinity inherent to the polysulfone (PSF) support material [71]. Additionally, the analysis identified distinct diffraction peaks at 2θ values of approximately 7.3°, 10.4°, and 12.9°, corresponding to the (011), (002), and (112) planes, respectively, which are characteristic of the crystalline structure of ZIF-8-NH_2 particles. These results are consistent with prior studies [1,72], confirming the effective incorporation of ZIF particles into the TFN membranes without significant loss of crystallinity.

Furthermore, Table 2 **and Fig. S5b** summarize the CO_2/CH_4 separation performance of the TFN membranes incorporating varying concentrations of ZIF-8-NH_2 (5, 10, and 15 wt%). As shown, the basic ST/PVA membrane (TFC-ST-1 %) with no MOF exhibits moderate selectivity, with CO_2 permeance of 212 GPU and CO_2/CH_4 selectivity of 17.3. Incorporating ZIF-8-NH_2 (5 wt%) into the TFN membrane enhances the separation performance, increasing the CO_2 permeance to 224 GPU, resulting in an improved CO_2/CH_4 selectivity of 21.1. This indicates that ZIF-8-NH_2 enhances CO_2 selectivity by facilitating CO_2 diffusion while limiting the CH_4 transport due to its strong affinity for CO_2 molecules, related to the molecular sieving effect and electrostatic attraction between the amine groups in the MOF and the CO_2 molecules [1]. Further increasing ZIF-8-NH_2 to (10 wt%) within (ST/PVA) TFN yields CO_2 permeance of 218 GPU, with CO_2/CH_4 selectivity improving to 22.3. This optimal balance suggests an effective dispersion of ZIF-8-NH_2, enhancing the separation performance without compromising the CO_2 permeability. At 15 wt% ZIF-8-NH_2 incorporation within the TFN membrane, the CO_2 permeance decreases slightly to 208 GPU, probably due to the barrier effect created by the high concentration of MOF particles strongly adhered to the polymer. However, the CO_2/CH_4 selectivity reaches its highest value of 26.9, indicating that higher filler content promotes the CO_2/CH_4 selectivity. Such a selectivity value almost doubles the selectivity obtained for dense blending biopolymer membranes. This study presents, for the first time, the successful application of a pure starch biopolymer membrane without blending. The formation of an ultrathin starch layer in both TFC and TFN configurations on porous support eliminates the need for a crosslinking agent, enhancing the membrane's environmental sustainability. This approach not only maintains structural integrity and performance but also reduces the use of chemical additives, making it a more eco-friendly alternative for gas separation applications.

The performance of thin-film nanocomposite (TFN) membranes based on starch/PVA without citric acid crosslinking was found to be significantly superior in terms of CO_2 separation. The optimized TFN membrane, containing 15 wt% NH_2-ZIF-8 and a ST/PVA ratio of 9/91, exhibited a CO_2 permeance of 208 GPU and a CO_2/CH_4 selectivity of 27. Therefore, a direct comparison between dense MMMs and TFC/TFN membranes should be made with caution, as these systems differ in selective layer thickness (~1 μm for TFC/TFNs vs. bulk dense films), starch/PVA composition, and crosslinking conditions. For example, at 9 % starch, a dense film crosslinked with 2 wt% citric acid showed a CO_2

Table 2
CO_2/CH_4 mixture separation performance for the PSF support and TFC membranes with different starch/PVA composition (0/100 to 100/0) and TFN membranes with the selected polymer concentrations comprising different ZIF-8-NH_2 loadings (5–15 wt%). Note that no crosslinker is needed for TFC/TFN membranes.

Membrane sample	ST/PVA composition	P_{CO2} (GPU)	P_{CH4} (GPU)	$S(CO_2/CH_4)$	CO_2 Purity (%)	CO_2 Recovery (%)
PSF (support)	–	411 ± 1	122 ± 1	3.4 ± 0.2	77.3	0.221
TFC.ST-0	0/100	96.5 ± 3.3	7.4 ± 0.2	13.0 ± 0.1	92.9	0.052
TFC.ST-9	**9/91**	**212 ± 8**	**12.3 ± 0.4**	**17.3 ± 0.2**	94.5	0.114
TFC.ST-17	17/83	157 ± 4	13.5 ± 0.2	11.6 ± 0.1	92.1	0.085
TFC.ST-23	23/77	93.5 ± 2.1	8.1 ± 0.2	11.6 ± 0.2	92.1	0.050
TFC.ST-33	33/67	66.1 ± 1.6	6.6 ± 0.1	10.1 ± 0.1	91.0	0.036
TFC.ST-100	100/0	61.6 ± 1.4	5.3 ± 0.1	11.7 ± 0.1	92.1	0.033
TFN ST-9-ZIF-8-NH_2 (5 wt%)	9/91	224 ± 4	10.2 ± 0.2	21.1 ± 1.0	95.5	0.121
TFN ST-9-ZIF-8-NH_2 (10 wt%)	9/91	218 ± 6	9.8 ± 0.5	22.3 ± 1.1	95.7	0.118
TFN ST-9-ZIF-8-NH_2 (15 wt%)	**9/91**	**208 ± 2**	**8.0 ± 1.7**	**26.9 ± 2.3**	96.4	0.112

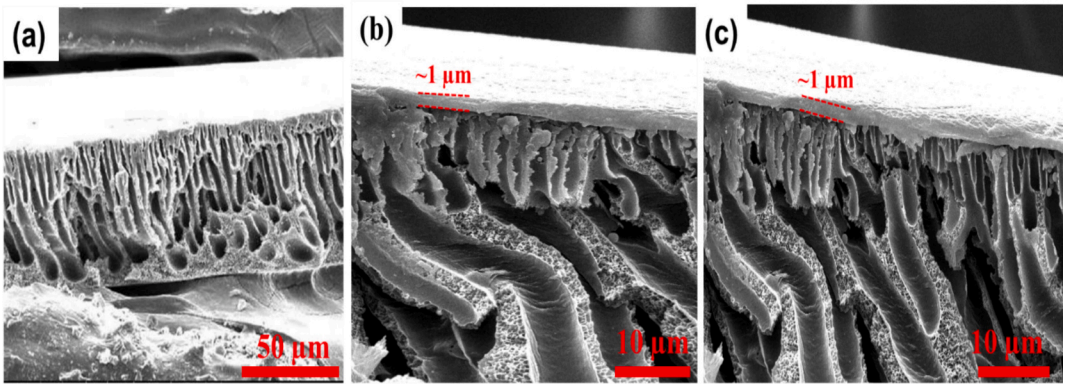

Fig. 9. SEM cross-section images for starch/PVA TFC membranes: PSF support (a); TFC.ST-9 (b); TFN ST-9-ZIF-8-NH_2 (10 wt%) (c).

permeability of 55.6 Barrer and selectivity of 10.5, whereas the corresponding non-crosslinked TFC membrane reached 212 Barrer with higher selectivity (17.3). At 33 % starch, however, the dense film (123.7 Barrer, 14.1) outperformed the TFC membrane (66.1 Barrer, 10.1). These observations highlight that separation performance results from the combined effects of composition, crosslinking, and membrane architecture rather than selective layer thickness alone. Overall, the preliminary work done with dense MMMs is not fully extrapolated to the preparation of TFN membranes but constitutes a useful guide for the synthesis and understanding of the basic phenomena related to both membrane fabrication and gas separation performance. In addition, the TFN design through its ultrathin selective layer and MOF incorporation provides a promising route to enhanced CO_2/CH_4 separation, although the optimum outcome strongly depends on blend composition and fabrication strategy.

This decline in performance is likely due to densification and reduced chain mobility resulting from citric acid crosslinking, which can restrict gas diffusion and potentially lead to microstructural defects. These results illustrate the critical influence of membrane thickness, crosslinking degree, and polymer-filler compatibility on gas transport properties. Excessive crosslinking, while beneficial for mechanical integrity, can compromise separation performance by reducing free volume and hindering diffusivity. These findings are consistent with previous reports [31,55,73] that highlight the trade-offs between permeability and selectivity in high free-volume or blended membrane systems.

The incorporation of citric acid as a crosslinker generally improved the CO_2/CH_4 separation performance of dense starch–PVA membranes. Specifically, the permeability reached its maximum at 2 wt% citric acid and then slightly decreased with further addition, while CO_2/CH_4 selectivity continued to increase. This behavior is consistent with the expected trade-off in dense polymeric membranes, where excessive

Table 3
Biopolymer and common conventional membranes applied in gas separations.

MMM		wt% loading (best performance)	Solvent	P CO_2 [a,b]	Sel. CO_2/CH_4	Sel. CO_2/N_2	Ref.
Biopolymer/conventional polymer	**filler**						
Pristine CA	–	–	NMP	15.5[a]	10.7	8.8	[53]
CA	NH_2-MIL-53(Al)	10, (15), 20		52.6[a]	28.7	23.4	[53]
CS/dialdehyde ST-	PVA	5,7.5, (10)	Glacial AcOH	–	–	19.8	[20]
Pristine CA	–	–		2.28[a]	–	25.5	[76]
CA	Co(II)–NaY	0, 5, 10, (15), 20	THF	3.28[a]	–	29.9	[76]
CA	NaY	0, 5, 10, 15, (20)		4.87[a]	–	25	[76]
CA/HFMs	CA	12, 14, 16, (18), 20, 22	NMP	1.26[a]	7.9	6.0	[77]
Pristine CNF	–	–	DI H2O,	4.58[a]	4.44	5.85	[78]
CNF	ZIF-8	10, 30, 50, (70), 90		550[a]	36.2	45.5	[78]
Carboxymethyl CS	PZ	(20), 30, 40	DI H_2O	89[b]	–	103	[79]
Carboxymethyl CS	dendrimer (PAMAM)	(10), 20, 30	–	98[b]	–	149	[80]
PVA	CNC	0.5, (1), 1.5, 2	DI H_2O	2.9[b]	43	–	[81]
Cellulose/ [Zn(II)24.2 %]	PEI-GO	10, 13, 16, (17), 18	DI H_2O	268.9[a]	57.4	48.9	[82]
CA	R-MWCNTs	0, (0.65), 1, 2	THF	–	13.41	9.33	[83]
CA	C-MWCNTs	0, (0.65), 1, 2	THF	–	21.81	15.43	[83]
CA	PEG/(C-MWCNT])	0, (0.5), 1, 2	THF	–	53.98	26.37	[83]
CA	SBR/(C-MWCNT)	0, 0.5, 1, (2)	THF	–	43.91	26.68	[83]
PIM-1	MOF-808	10	$CHCl_3$	9090[a]	16.2	–	[84]
PIM-1	MXene	5	$CHCl_3$	7652[a]	13.5	–	[85]
Matrimid	ZIF-8	20	$CHCl_3$	20[a]	44	–	[86]
Matrimid	MIL-53	15	NMP	12[a]	52	–	[87]
P84	$Ni_3(HCOO)_6$	15	NMP	1.26[a]	67	–	[88]
P84	ZIF-8	27	DMF	11[a]	93	–	[89]
ST/PVA (33/67)/citric acid	**ZIF-8-NH_2**	**5, (10), 15**	**DI H_2O**	**188**[a]	**16.5**	**–**	**This work**
ST/ PVA(9/91)	**ZIF-8-NH_2**	**5, 10, (15)**	**DI H_2O**	**217.9**[b]	**22.3**	**–**	**This work**

Abbreviations. Polymers: CA (Cellulose acetate), CS (Chitosan), ST (Starch), PVA (Polyvinyl alcohol), CNF (cellulose nanofiber). Solvents: NMP (1-Methyl-2-Pyrrolodone), AcOH (acetic acid), DMF (*N*, *N*-dimethylformamide), THF (Tetrahydrofuran), CF (Chloroform), DI H_2O (Deionized water).
(–) Not tested.
[a] Permeability in Barrer unit (1 Barrer = 3.35×10^{-16} mol·m^{-2}·s^{-1}·Pa^{-1}). 1 Barrer can be also expressed as 10^{-10} cm^3(STP)·cm·cm^{-2}·s^{-1}·cm·Hg^{-1}.
[b] Permeance given in Gas Permeability Unit (GPU) (1 GPU = 3.35×10^{-10} mol·m^{-2}·s^{-1}·Pa^{-1}). 1 GPU can be also expressed as 10^{-6} cm^3(STP) ·cm^{-2}·s^{-1}·cm·Hg^{-1}.

crosslinking restricts chain mobility and reduces gas diffusion. In terms of composition, the optimum performance for dense membranes was obtained with a 33/67 starch–PVA blend, whereas in TFC membranes the best separation efficiency occurred at a much lower starch content (9/91 ST–PVA). This difference highlights the role of membrane architecture: dense films require higher starch content to enhance CO_2 sorption, while in ultrathin TFC selective layers the support provides mechanical stability, enabling a small starch fraction to introduce CO_2-philic sites while the higher PVA content ensures continuity and minimizes defects.

Furthermore, Table 3 compares our best-performing polysaccharide membranes with other biopolymer membranes in the literature [74,75]. It provides a comparative analysis of various MMMs for CO_2 separation, highlighting differences in polymer-filler systems, solvent selection, gas permeability/permeation, and selectivity. It demonstrates how different biopolymer matrices, such as cellulose acetate (CA), chitosan (CS), polyvinyl alcohol (PVA), and starch/PVA, impact gas separation performance [74,75]. The incorporation of nanofillers, including MOFs (e.g., NH_2-MIL-53(Al), ZIF-8) and carbon-based materials, enhances CO_2 transport by improving sorption sites and diffusion pathways. CO_2 Permeability varies widely depending on the polymer-filler combination. CA-based membranes generally exhibit lower permeability values (2–52 Barrer), whereas CNF-ZIF-8 membranes demonstrate permeability as high as 550 Barrer, illustrating the strong impact of MOFs on enhancing gas transport. CO_2/CH_4 selectivity ranges from 7.9 to 57.4, emphasizing the role of functionalized fillers in improving membrane selectivity. Higher selectivity is essential for efficient CO_2 separation in natural gas processing and biogas upgrading. The results indicate that starch/PVA MMMs with ZIF-8-NH_2 exhibit superior CO_2 permeability (188 Barrer) and CO_2/CH_4 selectivity (22.3) compared to many conventional biopolymer-based MMMs. Thin-film nanocomposite (TFN) membranes achieve CO_2 permeance of 217.9 GPU, confirming their efficiency. Unlike conventional membranes requiring chemical crosslinking, starch/PVA TFN membranes offer an environmentally friendly alternative, eliminating the need for additional crosslinking agents while maintaining high performance. The amino-functionalized NH_2-ZIF-8 enhances interfacial compatibility and selective CO_2 transport, making these membranes promising candidates for sustainable gas separation applications.

Additionally, the performance of the developed starch/PVA-based TFC and TFN membranes was compared with state-of-the-art integrally skinned asymmetric polysulfone (PSf) membranes, which are among the most widely studied polymer membranes for CO_2/CH_4 separation. Although PSf is valued for its robustness and ease of processing, its intrinsic gas separation properties are limited. Reported data for asymmetric PSf membranes typically show CO_2 permeance in the range of ~5–10 GPU with CO_2/CH_4 selectivity between 10 and 15 under biogas upgrading condition [4,90–92]. Such performance is insufficient to achieve the required recovery and purity levels for industrial upgrading without blending or further modification. By contrast, the best-performing TFN membrane in this work exhibited a CO_2 permeance of ~208 GPU and a CO_2/CH_4 selectivity of ~27, representing more than an order of magnitude increase in permeance together with substantially higher selectivity. This comparison underscores the advantage of employing renewable starch/PVA matrices combined with MOF fillers in thin selective layers, which not only surpass the intrinsic separation limits of conventional PSf membranes but also provide a more sustainable alternative.

Additionally, as shown in Table 3, the developed starch/PVA and ST/PVA/citric acid MMMs were evaluated against several well-known common polymeric and MMMs reported in the literature. For example, PIM-1-based MMMs, such as those with MOF-808 [84] or MXene fillers [85], exhibit very high CO_2 permeability values (9090 and 7652 Barrer, respectively), but with moderate CO_2/CH_4 selectivity values (16.2 and 13.5). However, these membranes are often prone to physical aging, which compromises their long-term performance [93]. Similarly, Matrimid®5218 MMMs filled with ZIF-8 [86] or MIL-53 [87] offer significantly lower permeability values (20 and 12 Barrer, respectively) but display higher selectivity (44 and 52), reflecting their more rigid and less permeable matrix. Pure Matrimid®5218, depending on the filler, can also show reduced plasticization resistance under realistic mixed-gas conditions. P84-based membranes also demonstrate selective CO_2/CH_4 separation, with CO_2 permeability values ranging from 1.26 to 11 Barrer and selectivities reaching up to 93, depending on the filler and formulation [88,89]. While the selectivity is high, the extremely low permeability limits their throughput and scalability for industrial applications. In contrast, our developed ST/PVA membranes filled with ZIF-8-NH_2 achieved a favorable balance between permeability and selectivity. Specifically, ST/PVA/citric acid MMMs with 10 wt% ZIF-8-NH_2 exhibited a CO_2 permeability of 188 Barrer and a CO_2/CH_4 selectivity of 16.5, while the ST/PVA MMMs with 15 wt% filler reached 218 Barrer and 22.3 selectivity. These results are comparable to or even superior to several conventional MMMs in terms of overall separation performance. Beyond separation efficiency, our membranes present important sustainability and practical advantages: they are derived from renewable starch, processed using water as a green solvent, and free from toxic crosslinkers or harsh organic solvents. Additionally, they maintain robust mechanical stability, making them a promising and eco-friendly alternative for CO_2/CH_4 separation in natural gas processing and carbon capture applications.

Furthermore, the separation performance data originally summarized in Table 3 have now been replotted in a Robeson-like plot, where CO_2/CH_4 selectivity is plotted against CO_2 permeance (Fig. 10). This graphical representation provides a clearer and more direct comparison between our fabricated membranes and those reported in the literature (as presented in Table 3), while Fig. 10 offers a visual overview that highlights the position of our membranes relative to both biobased and conventional membranes. The comparison confirms that our membranes exhibit CO_2 permeance and CO_2/CH_4 selectivity within the range of previously reported results, demonstrating their competitiveness and potential for gas separation applications.

Finally, the hydrophilic nature of starch means that exposure to humidity can lead to significant plasticization, as water molecules disrupt hydrogen bonding within the polymer matrix and increase chain mobility [94,95]. In membrane operation, such plasticization may result in increased CO_2 and CH_4 permeability but reduced CO_2/CH_4 selectivity, as the polymer matrix becomes less rigid and non-selective diffusion pathways are enhanced. Biogas streams are typically saturated with water vapor; although pre-treatment by cooling and

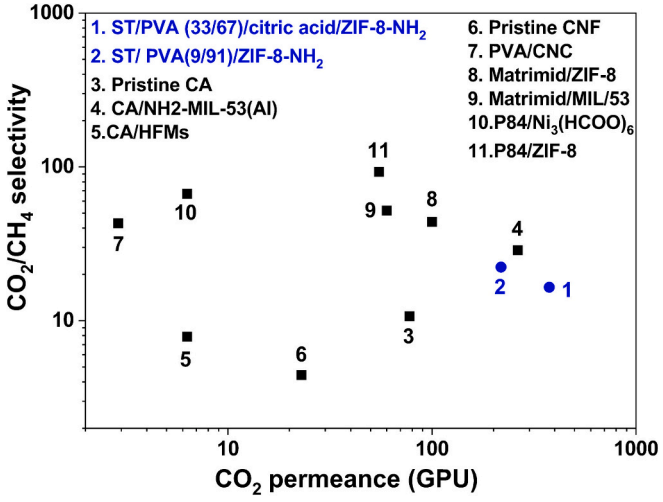

Fig. 10. CO_2/CH_4 separation selectivity as a function of CO_2 permeance for the membranes developed in this work, compared with reported biobased and conventional membranes (data from Table 3).

adsorption substantially reduces water content, residual humidity is still expected [96,97]. Therefore, the membranes developed here may experience altered performance under humid conditions compared to the dry-gas measurements reported. The incorporation of PVA and citric acid crosslinking was designed in part to mitigate this effect (have in mind that the amount of starch in the optimum membrane is relatively low, i.e. 9 %), since both strategies reduce the free volume available for water sorption and improve dimensional stability [22]. Furthermore, the addition of ZIF-8-NH_2 nanoparticles may provide additional water-resistance benefits by introducing rigid crystalline domains that help restrict excessive swelling [23]. Future work should evaluate the separation performance of these membranes under controlled humidified gas feeds to quantify the extent of humidity-induced plasticization, together with more realistic separation conditions to further optimize membrane formulations for practical biogas upgrading applications.

4. Conclusions

This study demonstrates the successful development of starch/PVA-based mixed-matrix membranes (MMMs) enhanced with ZIF-8-NH_2 fillers for efficient CO_2/CH_4 separation, presenting both scientific innovation and practical relevance. The pristine dense starch/PVA (33/67) membrane achieved a baseline CO_2 permeability of 124 Barrer with a selectivity of 14.0. Incorporation of ZIF-8-NH_2 fillers at optimized loadings (5, 10 and 15 wt%) significantly improved the gas separation performance, with 10 wt% loadings yielding the highest CO_2 permeability of 188 Barrer and a selectivity of 16.5. This enhancement can be attributed to the tailored microporosity, high specific surface area and amino-functionalized structure of ZIF-8-NH_2, which facilitated selective CO_2 adsorption and diffusion mechanisms. The transition from dense membranes to thin-film composite (TFC) and thin-film nanocomposite (TFN) membranes further substantiated the scalability and practical viability of this system. TFC and TFN membranes achieved remarkable CO_2 permeance values of up to 208 GPU, corresponding to a CO_2/CH_4 selectivity of 26.9, surpassing the dense membrane performance while maintaining robust mechanical and structural integrity. These advancements reflect the adaptability of the fabrication process of biopolymer-based membranes toward industrial configurations. Key insights include the pivotal role of the filler-polymer interaction and the positive influence of ZIF-8-NH_2 on the polymer matrix. The amino-functional groups on ZIF-8-NH_2 promoted a stronger interfacial bonding, reducing defects and improving compatibility with the starch/PVA matrix. This synergy mitigated common challenges such as filler aggregation and void formation, ensuring a uniform filler dispersion and enhancing the CO_2/CH_4 separation efficiency. Additionally, polymer cross-linking further stabilized the dense matrix, contributing to the durability and gas transport performance of the membranes, but was not required when preparing thin films, minimizing the amount of the final material.

While this work focused on binary CO_2/CH_4 mixtures as a model system to establish baseline performance, the findings are directly relevant to natural gas upgrading and biogas purification, where CO_2 is the dominant impurity. In practice, industrial gas streams often contain additional components such as water vapor, hydrogen sulfide (H_2S), nitrogen, and light hydrocarbons. These components affect the membrane separation performance through competitive sorption or polymer plasticization. However, the hydrophilic and chemically tunable nature of starch/PVA-based matrices, combined with the selective affinity of amino-functionalized ZIF-8 toward CO_2, offers a promise for selective separation even in more complex gas mixtures.

Future work should therefore expand the scope of testing to include multicomponent feed gases and investigate membrane performance under realistic industrial conditions (e.g., presence of moisture, pressure fluctuations, and chemical contaminants). Long-term stability assessments and pilot-scale testing will also be crucial for translating this technology from laboratory-scale demonstration to real-world application.

Finally, this work highlights the potential of integrating renewable polymers, such as starch and PVA, with advanced functionalized and CO_2-philic fillers like ZIF-8-NH_2 to create sustainable and high-performance gas separation solutions based on membranes. Future investigations should focus on refining filler dispersion methods, exploring novel functionalized MOFs, using a full renewable composition from the support to the skin layer, and conducting long-term operational studies under industrially relevant conditions, including higher feed compositions and the absence of sweep gas, to validate the scalability and real-world applicability. This approach represents a significant step forward in addressing global challenges in carbon capture and natural gas purification while promoting eco-friendly and sustainable technologies.

CRediT authorship contribution statement

Dalia Refaat: Writing – original draft, Supervision, Methodology, Investigation, Conceptualization. **Jacking Amenakpor:** Methodology, Investigation. **Joaquín Coronas:** Writing – review & editing, Supervision, Funding acquisition. **Beatriz Zornoza:** Writing – review & editing, Supervision, Methodology, Funding acquisition, Conceptualization.

Declaration of competing interest

The authors declare that they have no known competing financial interests or personal relationships that could have appeared to influence the work reported in this paper.

Acknowledgements

B. Zornoza acknowledges the grant RYC2022-038139-I funded by MICIU/AEI/10.13039/501100011033 and ESF+. This work was supported by grants PID2022-138582OB-I00 (funded by MCIN/AEI/10.13039/501100011033 and "ERDF A way of making Europe"), TED2021-130621B-C4 (funded by MCIN/AEI/10.13039/501100011033 and the European Union-Next Generation EU), and CEX2023-001286-S (funded by MICIU/AEI/10.13039/501100011033). Financial assistance was also provided by the Government of Aragon (T68_23R). The authors would like to thank the Universidad de Zaragoza for the use of "Servicio General de Apoyo a la Investigación-SAI" and the use of instrumentation as well as the technical support and access to the National Facility ELECMI ICTS, "Laboratorio de Microscopias Avanzadas", at the "Universidad de Zaragoza". Finally, J. Amenakpor thanks the European Commission - Education, Audiovisual and Culture Executive Agency (EACEA) for the Erasmus Mundus scholarship under the program: Master in Membrane Engineering for Sustainable Development, MESD, Project number: 101081874, Call: ERASMUS-EDU-2022-PEX-EMJM-MOB.

Appendix A. Supplementary data

Supplementary data to this article can be found online at https://doi.org/10.1016/j.seppur.2025.135596.

References

[1] D. Refaat, M. Yahia, J. Coronas, Thin film nanocomposite membranes based on renewable polymer Pebax® and zeolitic imidazolate frameworks for CO2/CH4 separation, Process Saf. Environ. Prot. 192 (2024) 401–411.
[2] M. Karaszova, B. Zach, Z. Petrusova, V. Červenka, M. Bobák, M. Šyc, P. Izak, Post-combustion Carbon Capture by Membrane Separation, Sep. Purif. Technol. 238 (2019) 116448.
[3] N. Saini, K. Awasthi, Insights into the progress of polymeric nano-composite membranes for hydrogen separation and purification in the direction of sustainable energy resources, Sep. Purif. Technol. 282 (2022) 120029.

[4] Y. Zhang, J. Sunarso, S. Liu, R. Wang, Current status and development of membranes for CO2/CH4 separation: A review, Intern. J. Greenhouse Gas Control 12 (2013) 84–107.
[5] B. Zornoza, A. Martinez-Joaristi, P. Serra-Crespo, C. Tellez, J. Coronas, J. Gascon, F. Kapteijn, Functionalized flexible MOFs as fillers in mixed matrix membranes for highly selective separation of CO2 from CH4 at elevated pressures, Chem. Commun. 47 (2011) 9522–9524.
[6] S. Saeed Mohammed, A. Qadir, Biopolymers: An Introduction and Biomedical Applications, J. Phys. Chem. Funct. Mater. 7 (2024).
[7] B.D. Freeman, Basis of Permeability/Selectivity Tradeoff Relations in Polymeric Gas Separation Membranes, Macromolecules 32 (1999) 375–380.
[8] L.M. Robeson, Correlation of separation factor versus permeability for polymeric membranes, J. Membr. Sci. 62 (1991) 165–185.
[9] B. Zornoza, C. Tellez, J. Coronas, J. Gascon, F. Kapteijn, Metal organic framework based mixed matrix membranes: An increasingly important field of research with a large application potential, Microporous Mesoporous Mater. 166 (2013) 67–78.
[10] L.M. Robeson, The upper bound revisited, J. Membr. Sci. 320 (2008) 390–400.
[11] F. Galiano, K. Briceño, T. Marino, A. Molino, K.V. Christensen, A. Figoli, Advances in biopolymer-based membrane preparation and applications, J. Membr. Sci. 564 (2018) 562–586.
[12] N.S.K. Gowthaman, H.N. Lim, T.R. Sreeraj, A. Amalraj, S. Gopi, Chapter 15 - Advantages of biopolymers over synthetic polymers: social, economic, and environmental aspects, in: S. Thomas, S. Gopi, A. Amalraj (Eds.), Biopolymers and their Industrial Applications, Elsevier, 2021, pp. 351–372.
[13] V. Vatanpour, B. Yavuzturk Gul, B. Zeytuncu, S. Korkut, G. İlyasoğlu, T. Turken, M. Badawi, I. Koyuncu, M.R. Saeb, Polysaccharides in fabrication of membranes: A review, Carbohydr. Polym. 281 (2022) 119041.
[14] R.P. Babu, K. O'Connor, R. Seeram, Current progress on bio-based polymers and their future trends, Prog Biomater 2 (2013) 8.
[15] T. Jiang, Q. Duan, Z. Jian, H. Liu, L. Yu, Starch-based Biodegradable Materials: Challenges and Opportunities, Adv. Indus. Eng. Polymer Res. 3 (2019).
[16] A. Zarei, V. Ghaffarian, Preparation and Characterization of Biodegradable Cellulose Acetate-Starch Membrane, Polym.-Plast. Technol. Eng. 52 (2013) 387–392.
[17] T.R. Arruda, G.D. Machado, C.S. Marques, A.L. Souza, F.M. Pelissari, T.V. Oliveira, R.R. Silva, An Overview of Starch-Based Materials for Sustainable Food Packaging: Recent Advances, Limitations, and Perspectives, Macromol, in, 2025.
[18] R. Abedi-Firoozjah, N. Chabook, O. Rostami, M. Heydari, A. Kolahdouz-Nasiri, F. Javanmardi, K. Abdolmaleki, PVA/starch films: An updated review of their preparation, characterization, and diverse applications in the food industry, Polym. Test. 118 (2022) 107903.
[19] S. Saedi, S.S. Madaeni, F. Seidi, A.A. Shamsabadi, S. Laki, Synthesis and application of a novel Amino-Starch derivative as a new polymeric additive for fixed facilitated transport of carbon dioxide through an asymmetric polyethersulfone (PES) membrane, Intern. J. Greenhouse Gas Control 19 (2013) 126–137.
[20] J. Ren, H. Xuan, L. Ge, Double network self-healing chitosan/dialdehyde starch-polyvinyl alcohol film for gas separation, Appl. Surf. Sci. 469 (2019) 213–219.
[21] A. Jimenez, M. Fabra, P. Talens, A. Chiralt, Edible and Biodegradable Starch Films: A Review, Food Bioprocess Technol. 5 (2012).
[22] I.S. Arvanitoyannis, E. Psomiadou, A. Nakayama, S.-I. Aiba, N. Yamamoto, Edible films made from gelatin, soluble starch and polyols, Part 3, Food Chem. 60 (1997) 593–604.
[23] L. Yu, K. Dean, L. Li, Polymer blends and composites from renewable resources, Prog. Polym. Sci. 31 (2006) 576–602.
[24] Y.U. Long, G. Christie, Microstructure and mechanical properties of orientated thermoplastic starches, J. Mater. Sci. 40 (2005) 111–116.
[25] S. Haouari, D. Rodrigue, A Low-Cost Porous Polymer Membrane for Gas Permeation, Materials, in, 2022.
[26] J. Ren, H. Xuan, L. Ge, Double network self-healing chitosan/ dialdehyde starch-polyvinyl alcohol film for gas separation, Appl. Surf. Sci. 469 (2018).
[27] M. Patil, S.N. Mathad, A.Y. Patil, M.N. Arshad, H.S. Alorfi, M. Puttegowda, A. M. Asiri, A. Khan, N. Azum, Synthesis and Characterization of Microwave-Assisted Copolymer Membranes of Poly(vinyl alcohol)-g-starch-methacrylate and Their Evaluation for Gas Transport Properties, Polymers, in, 2022.
[28] I.S. Arvanitoyannis, Totally and Partially Biodegradable Polymer Blends Based on Natural and Synthetic Macromolecules: Preparation, Physical Properties, and Potential as Food Packaging Materials, J. Macromolecular Science-reviews in Macromolecular Chemistry and Physics 39 (1999) 205–271.
[29] C. Amri, M. Mudasir, D. Siswanta, R. Roto, In vitro hemocompatibility of PVA-alginate ester as a candidate for hemodialysis membrane, Int. J. Biol. Macromol. 82 (2015).
[30] I. Dudeja, R.K. Mankoo, A. Singh, J. Kaur, Citric acid: An ecofriendly cross-linker for the production of functional biopolymeric materials, Sustain. Chem. Pharm. 36 (2023) 101307.
[31] P.S. Tin, T.S. Chung, Y. Liu, R. Wang, S.L. Liu, K.P. Pramoda, Effects of cross-linking modification on gas separation performance of Matrimid membranes, J. Membr. Sci. 225 (2003) 77–90.
[32] L. Martínez-Izquierdo, C. Téllez, J. Coronas, Highly stable Pebax® Renew® thin-film nanocomposite membranes with metal organic framework ZIF-94 and ionic liquid [Bmim][BF4] for CO2 capture, J Mater Chem A 10 (2022) 18822–18833.
[33] X. Wang, Y. Zhang, X. Chen, Y. Wang, M. He, Y. Shan, Y. Li, F. Zhang, X. Chen, H. Kita, Preparation of Pebax 1657/M7AF-7 Mixed Matrix Membranes with Enhanced CO_2/N_2 Separation by Active Site of Triazole Ligand, Membranes 12 (2022) 786.
[34] H. Li, Q. Zhu, Y. Dong, P. Zuo, Z. Yang, T. Xu, Ultra-microporous anion conductive membranes for crossover-free pH-neutral aqueous organic flow batteries, J. Membr. Sci. 668 (2023) 121195.
[35] K.S. Park, Z. Ni, A.P. Côté, J.Y. Choi, R. Huang, F.J. Uribe-Romo, H.K. Chae, M. O'Keeffe, O.M. Yaghi, Exceptional chemical and thermal stability of zeolitic imidazolate frameworks, Proc. Natl. Acad. Sci. 103 (2006) 10186–10191.
[36] D. Madhav, M. Malankowska, J. Coronas, Synthesis of nanoparticles of zeolitic imidazolate framework ZIF-94 using inorganic deprotonators, New J. Chem. 44 (2020) 20449–20457.
[37] W. Morris, N. He, K.G. Ray, P. Klonowski, H. Furukawa, I.N. Daniels, Y. A. Houndonougbo, M. Asta, O.M. Yaghi, B.B. Laird, A Combined Experimental-Computational Study on the Effect of Topology on Carbon Dioxide Adsorption in Zeolitic Imidazolate Frameworks, J. Phys. Chem. C 116 (2012) 24084–24090.
[38] P. Tanvidkar, S. Appari, B.V.R. Kuncharam, A review of techniques to improve performance of metal organic framework (MOF) based mixed matrix membranes for CO2/CH4 separation, Rev. Environ. Sci. Biotechnol. 21 (2022) 539–569.
[39] D. Fairen-Jimenez, S.A. Moggach, M.T. Wharmby, P.A. Wright, S. Parsons, T. Düren, Opening the Gate: Framework Flexibility in ZIF-8 Explored by Experiments and Simulations, J. Am. Chem. Soc. 133 (2011) 8900–8902.
[40] Y. Xiong, N. Deng, X. Wu, Q. Zhang, S. Liu, G. Sun, De novo synthesis of amino-functionalized ZIF-8 nanoparticles: Enhanced interfacial compatibility and pervaporation performance in mixed matrix membranes applying for ethanol dehydration, Sep. Purif. Technol. 285 (2022) 120321.
[41] J.A. Thompson, N.A. Brunelli, R.P. Lively, J.R. Johnson, C.W. Jones, S. Nair, Tunable CO2 Adsorbents by Mixed-Linker Synthesis and Postsynthetic Modification of Zeolitic Imidazolate Frameworks, J. Phys. Chem. C 117 (2013) 8198–8207.
[42] K. Pal, A. Banthia, D. Majumdar, Preparation of transparent starch based hydrogel membrane with potential application as wound dressing, Trends Biomater, Artif. Organs 20 (2006) 59–67.
[43] J.A. Thompson, C.R. Blad, N.A. Brunelli, M.E. Lydon, R.P. Lively, C.W. Jones, S. Nair, Hybrid Zeolitic Imidazolate Frameworks: Controlling Framework Porosity and Functionality by Mixed-Linker Synthesis, Chem. Mater. 24 (2012) 1930–1936.
[44] N. Singha, Starch-based blends and composites, 2021, p. 205.
[45] F. Cacho-Bailo, C. Téllez, J. Coronas, Interactive Thermal Effects on Metal–Organic Framework Polymer Composite Membranes, Chemistry – A, Eur. J. Dermatol. 22 (2016) 9533–9536.
[46] R. Jin, Z. Bian, J. Li, M. Ding, L. Gao, ZIF-8 crystal coatings on a polyimide substrate and their catalytic behaviours for the Knoevenagel reaction, Dalton Trans. 42 (2013) 3936–3940.
[47] H. Tian, J. Yan, V.R. Anumakonda, A. Xiang, X. Luo, Fabrication and properties of polyvinyl alcohol/starch blend films: Effect of composition and humidity, Int. J. Biol. Macromol. 96 (2016).
[48] E. Popa, M. Popa, M. Răpă, O. Popa, Preparation and characterization of biopolymer blends based on polyvinyl alcohol and starch, Romanian, Biotechnol. Lett. 20 (2015) 10306–10315.
[49] Q. Yuan, G. Zhu, A review on metal organic frameworks (MOFs) modified membrane for remediation of water pollution, Environ. Eng. Res. 26 (2021) 190435.
[50] W. Fan, X. Wang, B. Xu, Y. Wang, D. Liu, M. Zhang, Y. Shang, F. Dai, L. Zhang, D. Sun, Amino-functionalized MOFs with high physicochemical stability for efficient gas storage/separation, dye adsorption and catalytic performance, J Mater Chem A 6 (2018) 24486–24495.
[51] P. Dole, C. Joly, E. Espuche, I. Alric, N. Gontard, Gas transport properties of starch based films, Carbohydr. Polym. 58 (2004) 335–343.
[52] A. Jana, A. Modi, Recent progress on functional polymeric membranes for CO2 separation from flue gases: A review, Carbon Capture Science & Technology 11 (2024) 100204.
[53] M. Mubashir, Y.F. Yeong, K.K. Lau, T.L. Chew, J. Norwahyu, Efficient CO2/N2 and CO2/CH4 separation using NH2-MIL-53 (Al)/cellulose acetate (CA) mixed matrix membranes, Sep. Purif. Technol. 199 (2018) 140–151.
[54] A. Torre-Celeizabal, C. Casado-Coterillo, A. Gomis-Berenguer, J. Iniesta, A. Garea, Chitosan-based mixed matrix composite membranes for CO2/CH4 mixed gas separation, Experimental characterization and performance validation, Separation and Purification Technology 325 (2023) 124535.
[55] H. Wu, Y. Lei, J. Lu, R. Zhu, D. Xiao, C. Jiao, R. Xia, Z. Zhang, G. Shen, Y. Liu, S. Li, M. Li, Effect of citric acid induced crosslinking on the structure and properties of potato starch/chitosan composite films, Food Hydrocoll. 97 (2019) 105208.
[56] A.C. Alavarse, E.C.G. Frachini, R.L.C.G. da Silva, V.H. Lima, A. Shavandi, D.F. S. Petri, Crosslinkers for polysaccharides and proteins: Synthesis conditions, mechanisms, and crosslinking efficiency, a review, Int. J. Biol. Macromol. 202 (2022) 558–596.
[57] S. Gawish, S. Abo El-Ola, A. Ramadan, A. El-Kheir, Citric Acid Used as a Crosslinking Agent for the Grafting of Chitosan onto Woolen Fabric, J. Appl. Polym. Sci. 123 (2012).
[58] S. Im, A. Mostafa, D.-H. Kim, Use of citric acid for reducing CH4 and H2S emissions during storage of pig slurry and increasing biogas production: Lab- and pilot-scale test, and assessment, Sci. Total Environ. 753 (2021) 142080.
[59] B. Prasad, R. Borgohain, B. Mandal, Advances in Bio-based Polymer Membranes for CO2 Separation, in (2019) 277–307.
[60] R. Lin, B. Villacorta Hernandez, L. Ge, Z. Zhu, Metal organic framework based mixed matrix membranes: an overview on filler/polymer interfaces, J Mater Chem A 6 (2018) 293–312.
[61] V. Muthukumaraswamy Rangaraj, M.A. Wahab, K.S.K. Reddy, G. Kakosimos, O. Abdalla, E.P. Favvas, D. Reinalda, F. Geuzebroek, A. Abdala, G.N. Karanikolos,

Metal Organic Framework - Based Mixed Matrix Membranes for Carbon Dioxide Separation, Recent Advances and Future Directions, Front Chem 8 (2020) 534.
[62] B. Arundhathi, M. Pabba, S.S. Raj, N. Sahu, S. Sridhar, Advancements in Mixed-Matrix Membranes for Various Separation Applications: State of the Art and Future Prospects, Membranes, in, 2024.
[63] W. Su, Y. Xiang, Y. Dai, Y. Wang, S. Zhong, J. Li, Challenges and recent advances in MOF-based gas separation membranes, Chem. Commun. 60 (2024) 7124–7135.
[64] Z. Niu, N. He, Y. Yao, A. Ma, E. Zhang, L. Cheng, Y. Li, X. Lu, Mixed matrix membranes for gas separations: A review, Chem. Eng. J. 494 (2024) 152912.
[65] S. Anastasiou, N. Bhoria, J. Pokhrel, G. Karanikolos, Metal Organic Framework Mixed Matrix Membranes for CO2 Separation, 2016.
[66] J. Dechnik, C.J. Sumby, C. Janiak, Enhancing Mixed-Matrix Membrane Performance with Metal–Organic Framework Additives, Cryst. Growth Des. 17 (2017) 4467–4488.
[67] A. Imtiaz, M.H.D. Othman, A. Jilani, I.U. Khan, R. Kamaludin, O. Samuel, ZIF-filler incorporated mixed matrix membranes (MMMs) for efficient gas separation: A review, J. Environ. Chem. Eng. 10 (2022) 108541.
[68] H. Aasadi, O. Alizadeh, A. Ramazani, F. Dorosti, A review on the effects of fillers on gas separation Mixed Matrix Membranes, Iranian J. Chem. Eng. (IJChE) 19 (2022) 3–28.
[69] M. Kattula, K. Ponnuru, L. Zhu, W. Jia, H. Lin, E.P. Furlani, Designing ultrathin film composite membranes: the impact of a gutter layer, Sci. Rep. 5 (2015) 15016.
[70] T. Li, Y. Pan, K.-V. Peinemann, Z. Lai, Carbon dioxide selective mixed matrix composite membrane containing ZIF-7 nano-fillers, J. Membr. Sci. 425–426 (2013) 235–242.
[71] P. Lu, S. Liang, T. Zhou, X. Mei, Y. Zhang, C. Zhang, A. Umar, Q. Wang, Layered double hydroxide/graphene oxide hybrid incorporated polysulfone substrate for thin-film nanocomposite forward osmosis membranes, RSC, Advances 6 (2016) 56599–56609.
[72] L. Nguyen, K. Le, A Zeolite Imidazolate Framework ZIF-8 Catalyst for Friedel-Crafts Acylation, Chin. J. Catal. 33 (2012) 688–696.
[73] J.D. Wind, C. Staudt-Bickel, D.R. Paul, W.J. Koros, The Effects of Crosslinking Chemistry on CO2 Plasticization of Polyimide Gas Separation Membranes, Ind. Eng. Chem. Res. 41 (2002) 6139–6148.
[74] L. Deng, T.-J. Kim, M. Sandru, M.-B. Hägg, PVA/PVAm Blend FSC Membrane for Natural Gas Sweetening, in: H.E. Alfadala, G.V. Rex Reklaitis, M.M. El-Halwagi (Eds.) Proceedings of the 1st Annual Gas Processing Symposium, Elsevier, Amsterdam, 2009, pp. 247–255.
[75] L. Deng, T.-J. Kim, M.-B. Hägg, Facilitated transport of CO2 in novel PVAm/PVA blend membrane, J. Membr. Sci. 340 (2009) 154–163.
[76] H. Sanaeepur, A. Kargari, B. Nasernejad, A.E. Amooghin, M. Omidkhah, A novel Co2+ exchanged zeolite Y/cellulose acetate mixed matrix membrane for CO2/N2 separation, J. Taiwan Inst. Chem. Eng. 60 (2016) 403–413.
[77] M. Mubashir, Y.F. Yeong, K.K. Lau, T.L. Chew, Effect of spinning conditions on the fabrication of cellulose acetate hollow fiber membrane for CO2 separation from N2 and CH4, Polym. Test. 73 (2019) 1–11.
[78] M. Jia, X.-F. Zhang, Y. Feng, Y. Zhou, J. Yao, In-situ growing ZIF-8 on cellulose nanofibers to form gas separation membrane for CO2 separation, J. Membr. Sci. 595 (2020) 117579.
[79] R. Borgohain, B. Prasad, B. Mandal, Synthesis and characterization of water-soluble chitosan membrane blended with a mobile carrier for CO2 separation, Sep. Purif. Technol. 222 (2019) 177–187.
[80] R. Borgohain, B., Mandal, pH responsive carboxymethyl chitosan/poly (amidoamine) molecular gate membrane for CO2/N2 separation, ACS Appl. Mater. Interfaces 11 (2019) 42616–42628.
[81] Z. Jahan, M.B.K. Niazi, M.-B. Hägg, Ø.W. Gregersen, Cellulose nanocrystal/PVA nanocomposite membranes for CO2/CH4 separation at high pressure, J. Membr. Sci. 554 (2018) 275–281.
[82] T. Hou, L. Shu, K. Guo, X.-F. Zhang, S. Zhou, M. He, J. Yao, Cellulose membranes with polyethylenimine-modified graphene oxide and zinc ions for promoted gas separation, Cellulose 27 (2020) 3277–3286.
[83] A. Moghadassi, Z. Rajabi, S. Hosseini, M. Mohammadi, Fabrication and modification of cellulose acetate based mixed matrix membrane: Gas separation and physical properties, J. Ind. Eng. Chem. 20 (2014) 1050–1060.
[84] M. Yahia, L.A. Lozano, J.M. Zamaro, C. Téllez, J. Coronas, Microwave-assisted synthesis of metal–organic frameworks UiO-66 and MOF-808 for enhanced CO2/CH4 separation in PIM-1 mixed matrix membranes, Sep. Purif. Technol. 330 (2024) 125558.
[85] M. Yahia, D. Refaat, J. Coronas, C. Tellez, Enhancing CO2/CH4 separation performance in PIM-1 based MXene nanosheets mixed matrix membranes, Sep. Purif. Technol. 356 (2025) 129825.
[86] A. Kertik, L.H. Wee, M. Pfannmöller, S. Bals, J.A. Martens, I.F.J. Vankelecom, Highly selective gas separation membrane using in situ amorphised metal–organic frameworks, Energy Environ. Sci. 10 (2017) 2342–2351.
[87] F. Dorosti, M. Omidkhah, R. Abedini, Fabrication and characterization of Matrimid/MIL-53 mixed matrix membrane for CO2/CH4 separation, Chem. Eng. Res. Des. 92 (2014) 2439–2448.
[88] L. Sheng, Y. Guo, D. Zhao, J. Ren, S. Wang, M. Deng, Enhanced CO2/CH4 separation performance of BTDA-TDI/MDI (P84) copolyimide mixed-matrix membranes by incorporating submicrometer-sized [Ni3(HCOO)6] framework crystals, J. Nat. Gas Sci. Eng. 75 (2020) 103123.
[89] A. Guo, Y. Ban, K. Yang, W. Yang, Metal-organic framework-based mixed matrix membranes: Synergetic effect of adsorption and diffusion for CO2/CH4 separation, J. Membr. Sci. 562 (2018) 76–84.
[90] S. Yousef, J. Šereika, A. Tonkonogovas, T. Hashem, A. Mohamed, CO2/CH4, CO2/N2 and CO2/H2 selectivity performance of PES membranes under high pressure and temperature for biogas upgrading systems, Environ. Technol. Innov. 21 (2021) 101339.
[91] Y.-W. Jeon, D.-H. Lee, Gas Membranes for CO2/CH4 (Biogas) Separation: A Review, Environ. Eng. Sci. 32 (2015) 71–85.
[92] H. Julian, I.J.I.J.E. Wenten, Polysulfone membranes for CO2/CH4 separation: State of the art 2 (2012) 484–495.
[93] B. Qiu, Y. Gao, P. Gorgojo, X. Fan, Membranes of Polymer of Intrinsic Microporosity PIM-1 for Gas Separation: Modification Strategies and Meta-Analysis, Nano-Micro Letters 17 (2025) 114.
[94] B. Priya, V.K. Gupta, D. Pathania, A.S. Singha, Synthesis, characterization and antibacterial activity of biodegradable starch/PVA composite films reinforced with cellulosic fiber, Carbohydr. Polym. 109 (2014) 171–179.
[95] K. Martinez Villadiego, M.J. Arias Tapia, J. Useche, D. Escobar Macías, Thermoplastic Starch (TPS)/Polylactic Acid (PLA) Blending Methodologies: A Review, J. Polym. Environ. 30 (2022) 75–91.
[96] A. Francisco López, T. Lago Rodríguez, S. Faraji Abdolmaleki, M. Galera Martínez, P.M. Bello Bugallo, From Biogas to Biomethane: An In-Depth Review of Upgrading Technologies That Enhance Sustainability and Reduce Greenhouse Gas Emissions, in: Applied Sciences, 2024.
[97] E. Esposito, L. Dellamuzia, U. Moretti, A. Fuoco, L. Giorno, J.C. Jansen, Simultaneous production of biomethane and food grade CO2 from biogas: an industrial case study, Energy Environ. Sci. 12 (2019) 281–289.